Evaluation of remote sensing soil moisture data products with a new approach to analyse footprint mismatch with in-situ measurements

Xie, Qiuxia; Jia, Li; Menenti, Massimo; Chen, Qiting; Bi, Jingxue; Chen, Yonghui; Wang, Chunmei; Yu, Xinju

Important note
To cite this publication, please use the final published version (if applicable).
Please check the document version above.

Evaluation of remote sensing soil moisture data products with a new approach to analyse footprint mismatch with in-situ measurements

Qiuxia Xie, Li Jia, Massimo Menenti, Qiting Chen, Jingxue Bi, Yonghui Chen, Chunmei Wang & Xinju Yu

View supplementary material

Published online: 10 Dec 2024.

Submit your article to this journal

Article views: 272

View related articles

View Crossmark data

ISDE   AIR   Taylor & Francis
Taylor & Francis Group

∂ OPEN ACCESS   Check for updates

Evaluation of remote sensing soil moisture data products with a new approach to analyse footprint mismatch with in-situ measurements

Qiuxia Xie[a], Li Jia[b], Massimo Menenti[b,c], Qiting Chen[b], Jingxue Bi[a], Yonghui Chen[a], Chunmei Wang[b] and Xinju Yu[a]

[a]School of Surveying and Geo-Informatics, Shandong Jianzhu University, Jinan, People's Republic of China; [b]Key Laboratory of Remote Sensing and Digital Earth, Aerospace Information Research Institute, Chinese Academy of Sciences, Beijing, People's Republic of China; [c]Delft University of Technology, Delft, The Netherlands

ABSTRACT

Global-scale surface soil moisture (SSM) products (e.g. SMAP L3.0, ASCAT V3.0, ESA/CCI V7.1 and GLDAS V2.2) are vital for applications in hydrology, climate variability, and agriculture. This study uses a new SSM evaluation approach by combining temporal evolution, Coefficient of Variation (CV), Cumulative Distribution Function (CDF), evaluation metrics, and Triple Collocation Analysis (TCA) to assess SSM accuracy and spatial–temporal variability, particularly the impact of footprint mismatch when comparing retrieved SSM with in-situ measurements. Results revealed significant spatial variability and seasonal patterns in SSM, as indicated by the CV values and temporal evaluations at different resampling scales. The variability captured by in-situ measurements was comparable to that of SSM products. The impact of footprint mismatch between in-situ measurements and data products, particularly for SMAP and ASCAT SSM, was more significant and led to substantial differences in evaluation metrics between smaller and larger spatial scales. TCA alone cannot reliably assess the accuracy of global-scale SSM products without in-situ SSM measurements. Overall, our findings highlight the critical role of footprint mismatch on the estimated accuracy of SSM products and underscore the need to combine multiple evaluations into an overall scoring indicator, as proposed in this study.

1. Introduction

Surface soil moisture (SSM) is integral to the global water cycle and energy exchange, rendering it a significant variable in research concerning water resource management, drought monitoring, flood forecasting, heatwave prediction, agricultural yield estimation, and more (Ray et al. 2017; Wang et al. 2022a; Xie et al. 2021; Zheng et al. 2022). Consequently, there is an urgent need to generate globally-scaled, spatiotemporally continuous distributed datasets of SSM with high accuracy (Cui et al. 2019; Yao et al. 2021). While in-situ SSM measurements offer highly accurate information, their limited coverage restricts the analysis of climate change impacts on ecosystem functioning

on a global scale (Kerr et al. 2016). In recent years, remote sensing satellite sensors and SSM retrieval algorithms have rapidly advanced as efficient methods for mapping global-scale SSM (Zheng et al. 2022). Compared to visible light and near-infrared remote sensing, active/passive microwave remote sensing is less affected by clouds and rain, exhibits strong penetration, and is more sensitive to variations in SSM, thereby emerging as a crucial technique for estimating global-scale SSM (Al-Yaari et al. 2014; Gruber et al. 2017; Kim et al. 2016; Xie et al. 2022). Presently, microwave remote sensing technology for SSM monitoring is considered the most effective method for obtaining large-scale and high-resolution SSM information, being the only technique capable of directly measuring the average absolute SSM value in space (Mohanty et al. 2017). Research on microwave SSM data products has demonstrated their capability to provide valuable information for various applications, but land surface properties such as vegetation and surface roughness can affect their accuracy and quality (Meng et al. 2022; Njoku and Chan 2006). Evaluation methods for SSM data products often include comparison with in-situ measurements and inter-comparison with other satellite-derived datasets to assess consistency and reliability (Li, Tang, and Hong 2018; Nichols 2011). To address disparities in spatial data, robust techniques are needed, utilising in-situ measurements for calibration and validation (Liu et al. 2021).

In the recent decades, satellites equipped with active/passive microwave sensors have been successfully launched (Table 1). Utilising the observation data from these satellite sensors and employing both active and passive microwave SSM inversion algorithms, a range of SSM products have been developed and released (Beck et al. 2021; Zheng et al. 2022). Most of these products are daily global-scale SSM datasets with a coarse grid resolution ($> = 9$ km). However, due to various error sources such as SM retrieval algorithms, sensor limitations, and environmental factors like vegetation cover, surface roughness, and atmospheric conditions, the quality of these SM products from different satellites varies significantly, each presenting its own set of advantages and disadvantages (Gruber et al. 2020; Zeng et al. 2015). Among these, the global-scale Advanced Scatterometer (ASCAT) SSM products, based on the Soil Water Index (SWI) retrieval algorithm, exhibit a higher spatial resolution of 0.1° and fewer SSM missing values compared to most SSM products with a spatial resolution of 25 km (Kim et al. 2018; Wagner et al. 2013). Similarly, the global-scale Soil Moisture Active Passive (SMAP) SSM product with a spatial resolution of 9 km is derived from the Single Channel Algorithm – Vertical polarisation (SCA-V) and has shown strong performance in both the United States and Spain (Colliander et al. 2021; Jackson et al. 2016). The European Space Agency/Climate Change Initiative (ESA/CCI) SSM product, with a spatial grid resolution of 0.25°, is developed using a combination of merging algorithms, including the error estimation method of Triple Collocation Analysis (TCA) method. This product integrates multiple global active and passive microwave SSM products, including the AMSR-E, Soil Moisture and Ocean Salinity (SMOS), ASCAT, SMAP, among others, and has become one of the more widely used global-scale SSM products (Dorigo et al. 2017; Gruber et al. 2017). Furthermore, the Global Land Data Assimilation System (GLDAS) SSM product, available at multiple spatial scales, has been used to validate SSM data derived from satellite observations and is commonly considered a reference source for evaluating satellite-based global SSM products (Amini et al. 2023). The GLDAS SSM product incorporates land surface models using model-derived data from satellite observations and assimilation datasets (Amini et al. 2023; Rodell et al. 2004; Wen et al. 2014). Before these SSM products can be effectively used, comprehensive evaluations are essential. Moreover, a thorough understanding of the error characteristics associated with these SSM products is imperative to enhance their application and accuracy (Dorigo et al. 2010; Wu et al. 2021).

Prior to evaluate global-scale SSM products using in-situ measurements, we need to characterise the variability captured by in-situ SSM measurements in space and time. Most evaluation studies have employed direct comparison with in-situ SSM measurements (Al-Yaari et al. 2019; Ma et al. 2019; Xing et al. 2021; Zeng et al. 2015). Such studies utilised in-situ measured SSM data from a station based on the station spatial representativeness, assuming the values of one station (or the mean values of multiple stations in the same pixel of satellite SSM products) represented

Table 1. Overview of main global daily satellite – and model-based surface soil moisture products (SGR: spatial grid resolution; SC: Spatial coverage; TR: Temporal resolution; TC: Temporal coverage; Ob. Time represents the local time of satellite overpass; LPRM: Land Parameter Retrieval Model; L-MEB: L-band Microwave Emission of The Biosphere; CLSM: Catchment Land Surface Model).

Products	Versions	Properties	SGR	SC	TR	TC (year)	Ob. Time	Units	Algorithms	References
AMSR-E	L3.0	Passive X-band	25 km	Global	Daily	2002~2011	01:30; 13:30	cm^3/cm^3	LPRM	(Owe, De Jeu, and Walker 2001)
AMSR-2	L3.0	Passive X-band	25 km	Global	Daily	2012~now	01:30; 13:30	cm^3/cm^3	LPRM	
FY3-B/C	L2.0	Passive X-band	25 km	Global	Daily	2011~now	01:40; 13:40	cm^3/cm^3	Qp	(Shi et al. 2006)
SMOS	L3.0	Passive L-band	25 km	Global	Daily	2010~now	06:00; 18:00	cm^3/cm^3	L-MEB	(Wigneron et al. 2007)
SMAP	L3.0	Passive L-band	9 km	Global	Daily	2015~now	06:00; 18:00	cm^3/cm^3	SCA-V	(Thomas J. Jackson 1993)
ASCAT	V3.0	Active C-band	0.10°	Global	Daily	2007~now	09:30; 21:30	%	TU-Wien	(Wagner, Lemoine, and Rott 1999)
ESA/CCI	V7.1	Merged product	0.25°	Global	Daily	1978~2020	08:00	cm^3/cm^3	TCA-based	(Bartalis et al. 2007)
GLDAS	V2.2	CLSM simulation	0.25°	Global	Daily	2003~now	08:00; 20:00	Kg/m^2	GLDAS-based	(Rodell et al. 2004)

the true value of the SSM product pixel (Cui et al. 2018; Karthikeyan et al. 2017a). This is a simple and easily executable approach. Karthikeyan et al. (2017a) evaluated 11 daily global-scale satellite SSM products, including ESA/ CCI, ASCAT, and SMAP, utilising in-situ measured SSM data obtained from the International Soil Moisture Network (ISMN) (Karthikeyan et al. 2017a). Their study suggested the necessity of establishing denser and multi-scale core observation networks or developing more robust evaluation techniques and methods to obtain more accurate evaluations of SSM products with global coverage (Karthikeyan et al. 2017b). If sufficient in-situ measured SSM data are available, the direct comparison with in-situ SSM measurements can yield relatively reliable evaluations of SSM products with coarse grid resolutions (Karthikeyan et al. 2017a). However, deploying a large number of ground stations with dense observation networks globally for SSM products with coarse grid resolution was deemed unrealistic, demanding considerable manpower, material, and financial resources (Dorigo et al. 2010). Limitations in the spatial coverage of in-situ stations and significant spatial scale disparities between in-situ SSM data and global-scale SSM products made obtaining dependable global evaluation results challenging (See Tables 1 and 2). To capture the spatial variability of global SSM – using in-situ measurements Xie et al. (2021) employed SSM data at three spatial scales: station-scale, airborne-1 km scale, and satellite-scale (>9 km), using airborne SSM data to elucidate the spatial heterogeneity of SSM within satellite pixels in highly heterogeneous areas (Xie et al. 2021). Their study indicated that fully exploiting the advantages of multi-source and multi-scale observation data held potential for enhancing the accuracy of satellite SSM products with coarse grid resolutions (> 9 km) (Menenti et al. 2021). Beck et al. (2021) discovered that spatial heterogeneity of SSM significantly impacted the accuracy of error estimation for SSM products with coarse grid scales ($\geq$ 9 km) when utilising in-situ SSM measurements (Beck et al. 2021).

In summary, the main issue in the evaluation of global-scale SSM products is whether in-situ measurements can be effectively used, notwithstanding the huge difference in the footprints of in-situ measurements and remote sensing data products. This leads to the main research question, which motivated this study: How to quantitatively evaluate the impact on the reliability of the SSM product assessment of the discrepancy between the footprints of in-situ measurements and data products by using in-situ measurements?

This question leads to identify four issues which need to be addressed systematically:

a) characterising the spatial and temporal variability of SSM captured by available in-situ measurements;
b) comparing the statistical distribution of in-situ and remote sensing SSM;
c) comparison of in-situ and remote sensing SSM at different grid-sizes;
d) global evaluation of remote sensing SSM using the TCA method;

Table 2. Overview of the in-situ soil moisture measurements used from ISMN in this study (N: the number of sites; SGR: spatial grid resolution; SC: Spatial coverage; TR: Temporal resolution; TC: Temporal coverage).

Names	Countries	Instruments	SGR	SC	TR	TC (yy.mm.dd)	N	References
CTP_SMTMN	China	5TM; EC-TM	Point	1.0°×1.0°	Hour	2010.08.01~2016.09.16	57	(Yang et al. 2013)
MAQU	China	ECH20; EC-TM	Point	3200 km²	Hour	2008.06.30~2010.07.31	20	(Su et al. 2011)
SMN-SDR	China	Decagon 5TM	Point	2.0°×2.0°	Hour	2018.07.25~2019.12.31	34	(Zhao et al. 2020)
HOBE	Denmark	Decagon 5TE	Point	2500 km²	Hour	2009.09.08~2019.03.13	32	(Bircher et al. 2012)
REMEDHUS	Spain	Stevens; Hydra Probe	Point	10000 km²	Hour	2005.03.15~2020.01.01	24	(Martínez-Fernández and Ceballos 2005)
OZNET	Australia	Stevens Hydra Probe;	Point	600 km², 2500 km²	Hour	2001.09.12~2018.08.27	20	(Young et al. 2008)
SASMAS	Australia	Stevens Hydra Probe; CS616	Point	40 km × 50 km	Hour	2005.12.31~2007.12.31	14	(Rüdiger et al. 2007)

1.1. Temporal evolution, spatial variability and Coefficient of Variation statistics of in-situ SSM measurements

Previous studies suggested that understanding the temporal evolution of SSM was vital for characterising hydrological cycles and land-atmosphere interactions. In-situ measurements and satellite retrievals often exhibited discrepancies in absolute values but may reveal consistent temporal patterns. Several studies have investigated temporal dynamics, demonstrating correlations and divergences between in-situ and satellite-derived SSM time series (Brocca et al. 2012; Cai et al. 2024; Herbert et al. 2020; Pandey and Pandey 2010; Weng et al. 2018). The Coefficient of Variation (CV) serves as a measure of relative variability within datasets (Jalilibal et al. 2021; Zhao et al. 2013). Assessing the CV of in-situ SSM measurements and satellite retrievals allows for the comparison of their variability despite differences in absolute values. Higher CV values indicate greater variability within the dataset. By analyzing the CV statistics, researchers can discern whether both observations capture similar degrees of variability over time and space. Previous studies have employed CV analysis to compare the variability of in-situ and satellite-derived SSM datasets, providing insights into their consistency and reliability (Sánchez et al. 2012; Zhao et al. 2013). While reconciling absolute SSM values between in-situ measurements and satellite retrievals remains challenging, identifying common temporal trends and variability patterns is crucial for advancing our understanding of SSM dynamics. By focusing on the temporal evolution and CV statistics of in-situ measurements, researchers aim to bridge the gap between these observational datasets. Such comparative analyses contribute to improving the accuracy and reliability of SSM observations, thereby facilitating better-informed decision-making in agriculture, water resource management, and climate modelling.

1.2. CDF comparison of in-situ and global-scale SSM data

To evaluate global-scale SSM products using in-situ measurements, we need to compare in detail the variability captured by in-situ measurements and remote sensing products. Research showed that comparing in-situ measurements with low-resolution microwave retrievals in SSM analysis poses challenges due to their inherent differences. Statistical comparison through (CDF) yields more meaningful interpretations (Brocca et al. 2011; Singh et al. 2020) . By analysing CDFs, we can discern the characteristics of both in-situ measurements and remote sensing data products, regardless of their absolute values (Kim et al. 2021b). This approach allows for a nuanced understanding of similarities, differences, and biases, thus facilitating a more accurate assessment of comparability and applicability. Many studies have used the CDF to analyze the differences between in-situ measurements and remote sensing data products. Further matching the CDF of remote sensing data with the measured data can be applied to improve the accuracy of rescaled remote sensing products (Gruber et al. 2013; Liu et al. 2011; Wang et al. 2022b). Liu et al. (2011) rescaled the ASCAT and ASMR-E SSM products against a reference land surface model data set using a CDF matching approach. Results showed the correlation coefficient between rescaled AMSR-E and ASCAT was greater than 0.65 against in situ SSM measurements, and demonstrated the advantages of CDF for the evaluation of remote sensing SSM products using in-situ SSM measurements (Liu et al. 2011). However, few studies have been conducted on the CDF comparability at different spatial scales between in-situ SSM measurements and remote sensing SSM product data.

1.3. Multi-spatial scale evaluation

The mismatch in the footprints of in-situ measurements and remote sensing data products is one of the important reasons for the unreliable evaluation results of global-scale SSM products using in-situ measurements (Colliander et al. 2018). The impact of spatial resolution on

comparing SSM retrievals with in-situ measurements extends beyond mere averaging of micro-wave (MW) signals in low-resolution satellite data (Colliander et al. 2018). While averaging certainly plays a role, the deeper reason lies in the non-linear relationship between MW emit-tance and SSM (Miralles, Crow, and Cosh 2010; Zwieback et al. 2016). This non-linearity com-plicates the inversion process, particularly when target properties are averaged before signal inversion, thus contributing to estimation errors. Understanding this complexity requires del-ving into the intricacies of SSM retrieval methodologies across different spatial scales. At finer resolutions, in-situ measurements capture localised variations in soil properties with high fidelity. However, the non-linear nature of MW emission – Soil Moisture relationships means that spatial averaging can obscure these fine-scale variations, leading to discrepancies when compared with in-situ data (Zwieback et al. 2016). Furthermore, the choice of retrieval algorithm and assimilation techniques also influences the impact of spatial resolution on retrie-val accuracy. Algorithms designed for coarse resolutions might employ different assumptions or parameterizations, further complicating comparisons with in-situ measurements. To address these challenges, researchers have developed a new evaluation approach that consider both the spatial resolution of satellite retrievals and the variability captured by in-situ measurements. This approach aims to quantify the error sources introduced by spatial averaging and non-lin-ear relationships, providing insights into the limitations of current SSM retrieval techniques (Colliander et al. 2018).

1.4. Global-scale evaluation using Triple Collocation Analysis (TCA) method

The TCA method derives error estimates from statistics of the differences between multiple data products, offering a robust approach to evaluate global-scale SSM retrievals (Kim, Dong, and Sharma 2021a; Lu et al. 2021; Wu et al. 2021). These studies employed three long time series pro-duct datasets to calculate errors for each of the three products without in-situ measurements, pro-ducing global error spatial distribution maps. For this method to work, each of the three product datasets needed over 100 sampling points and had to satisfy the following assumptions: each pro-duct's retrieval values are linearly related to the true SSM values; errors are zero-mean, mutually independent, and uncorrelated with errors of the other products; and errors are uncorrelated with the true SSM values (Chen et al. 2018; Hu et al. 2022; Xie et al. 2022). In theory, the TCA method can estimate the error statistics, including random and systematic errors, inherent in each dataset at a large spatial scale without requiring a single high-quality reference data, making it widely applicable in evaluating satellite – and model-based SSM products with coarse grid res-olutions. TCA provides a comprehensive understanding of the uncertainties associated with SSM retrievals, enabling researchers to better assess the reliability and accuracy of global-scale datasets. However, studies such as Kim et al. (2020) highlighted significant biases in estimated errors due to error cross-correlation in SSM product datasets (Kim et al. 2020). Gruber et al. (2016) also pointed out difficulties in fully satisfying the assumptions of the TCA method, even with SSM product data-sets obtained using different satellite sensor observation data and SSM inversion methods (Gruber et al. 2016). Although the TCA-based evaluation method can estimate errors of SSM products at a large spatial scale, the reliability in estimated errors remains to be investigated. Moreover, limited researches have been conducted on the inter-comparison of errors estimated based on in-situ measurements and TCA evaluation algorithms for remote sensing SSM products with coarse grid resolutions (> 9 km) (Zheng et al. 2022).

In this study we selected four global-scale SSM products, i.e. ASCAT (active microwave) with a spatial resolution of 0.1°, SMAP (passive microwave) with a spatial resolution of 9 km, ESA/CCI (active–passive merged product) with a spatial resolution of 0.25°, and GLDAS (model simu-lation) with a spatial resolution of 0.25°, to assess and understand the discrepancy between the footprints of in-situ measurements and remote sensing data products. This study introduced a comprehensive approach by combining temporal evolution analysis, CV statistics, CDF

comparison, evaluation metrics and the TCA method. This approach ensures a comprehensive assessment of the impact of footprint mismatches, providing valuable insights into the accuracy and variability of soil moisture data across different spatial scales. We believe this methodology effectively captures the complexities involved and enhances the reliability of the evaluation process. The paper is structured as follows: Section 2 provides detailed information on global-scale SMAP, ASCAT, ESA/CCI, and GLDAS SSM products (section 2.1), as well as in-situ SSM measurements from seven multi-spatial scale observation networks (section 2.2). The preprocessing details of these data are provided in section 2.3. Section 3 introduces the methodology, encompassing temporal evolution, CV, CDF, evaluation metrics, and the TCA method. Section 4 presents detailed analyses and evaluation results for SMAP, ASCAT, ESA/CCI, and GLDAS SSM products, including the analysis of SSM variability in space and time through temporal evaluations and CDF comparisons of in-situ and global-scale SSM data, along with evaluation and comparison results using error metrics and TCA methods respectively. Finally, the discussions and main conclusions are drawn in section 5 and 6.

2. Data collection and preprocessing

2.1. Global soil moisture products

This study utilised four global-scale daily soil moisture datasets, including data from NASA's SMAP mission, launched in 2015, which provides L-band radar and radiometer data. The focus is on the SMAP Level 3 product with a 9 km resolution, available from 2015 onwards. It also includes C-band radar data from the ASCAT sensors on ESA's MetOp satellites, using the 0.1° resolution product available since 2007, particularly the $T = 1$ layer representing soil depths of 1–5 cm. The study further incorporates the ESA/CCI V7.1 soil moisture product, which combines active and passive microwave data from 1978 to 2020, offering a global dataset with 0.25° resolution. Additionally, NASA's GLDAS V2.2 product, which integrates GRACE data since 2003, provides daily soil moisture data at a 0.25° resolution, focusing on the 0–2 cm soil layer. These datasets were used to assess the performance of different soil moisture products. Table 1 summarises their characteristics of these four global-scale daily soil moisture datasets assessed in this study. More details are provided in Appendix A.

2.2. In-situ measurements

The ISMN was established in 2009 through international collaboration (Beck et al. 2021; Karthikeyan et al. 2017a). Its aim was to create, maintain, and share a global in-situ soil moisture database for the evaluation and enhancement of global satellite products (such as SSM products and other land surface products) as well as hydrological models. Presently, the ISMN contains 65 in-situ observation networks comprising a total of 2678 sites, encompassing over 10,000 soil moisture data points (Dorigo et al. 2021). Although the ISMN constitutes a global observation network, most in-situ observation networks consist of single-station observations (Dorigo et al. 2011; Dorigo et al. 2021). Consequently, due to the substantial spatial variability of soil moisture, deriving reliable evaluations of global SSM products with coarse-grid spatial resolutions using these single-station observation network data has proven challenging. To address this challenge and examine the spatiotemporal variability of global-scale daily SSM products, we selected seven multi-scale in-situ observation networks that captured soil moisture variability across different spatial scales and geographic regions. These networks, covering diverse climatic and topographical conditions, provide high quality data that has undergone rigorous quality control and long term continuous monitoring. This study used data from these networks, collected during the period 2001–2020, to evaluate the global daily SMAP, ASCAT, ESA/CCI and GLDAS SSM products at different coarse grid resolutions (9 km, 0.1° and 0.25°) (Table 2).

2.2.1. CTP_SMTMN, MAQU, and SMN-SDR networks

Most in-situ stations of CTP_SMTMN, MAQU, and SMN-SDR networks are situated in grassland areas, while some are located in shrublands. All three observation networks are positioned in the Tibetan Plateau of China, covering approximately 100km × 100 km at an elevation of around 5000 m (Qin et al. 2013; Su et al. 2011; Zhao et al. 2020). The terrain is relatively flat, although there are numerous hills and valleys. The climate is typical of a semiarid monsoon climate, characterised by simultaneous rain and heat during certain periods; summers are hot and wet, while winters are cold and dry. The annual precipitation averages around 400–500 mm, with three-quarters occurring in the monsoon season from May to October (Yang et al. 2013). Following the monsoon, the surface gradually dries and freezes in winter, resulting in a high seasonal dynamic range of SSM content: low in spring and autumn, high in summer, and frozen in winter (Zhao et al. 2020).

2.2.2. REMEDHUS and HOBE networks

The REMEDHUS network is established by the Centro Hispano Luso de Investigaciones Agrariras (CIALE) at the Universidad de Salamanca, is positioned in the central sector of the Duero basin in Spain (Martínez-Fernández and Ceballos 2005). The climate in this region typifies a continental semi-arid Mediterranean climate, with an annual rainfall of about 385 mm and an average yearly temperature of approximately 12°C. Maximum precipitation occurs in May, while August witnesses the lowest levels (González-Zamora et al. 2019). The HOBE network, established in 2009, spans an area of 50 km × 50 km within the Ahlergaarde sub catchment of the Skjern catchment in western Denmark (Bircher et al. 2012). The topography is relatively flat, with surface elevations below 125 metres, and the predominant land use is agriculture (González-Zamora et al. 2015). Due to the sandy soil characteristics, occasional agricultural irrigation takes place. The climate, influenced by frequent rainfall from weather systems originating in the Atlantic Ocean, sees an average annual precipitation of about 1050 mm. The highest precipitation occurs from October to December, while April and May have the least rainfall (Ceballos et al. 2005; Sánchez et al. 2012; Sánchez et al. 2018).

2.2.3. OZNET and SASMAS networks

They are positioned in the Murrumbidgee River and Goulburn River catchments in southern New South Wales, Australia, established in 2001 and 2002, respectively (Rüdiger et al. 2007; Smith et al. 2012; Young et al. 2008). The climate in the Murrumbidgee Catchment ranges from semi-arid to humid, representing conditions typical of much of temperate Australia. The 20 in-situ stations of the OZNET networks are spread across two areas: the Yanco region with approximately 13 sites covering an area of around 2500 km^2, primarily comprising irrigation croplands, and the Kyeamba region with about 7 sites over a medium to small catchment of approximately 600 km^2, characterised by gentle slopes and mainly used for grazing (Young et al. 2008). The Goulburn River catchment extends from floodplains to around 1300 m in the northern and southern mountains. The climate here is subhumid or temperate, with an average annual rainfall of about 650 mm concentrated from November to March. Summer temperatures reach around 30°C, while winter temperatures hover at approximately 14°C (Smith et al. 2012).

These seven observation networks (CTP_SMTMN, MAQU, SMN-SDR, REMEDHUS, HOBE, OZNET and SASMAS) were initially set as multi-scale observation networks for validation of remote sensing data with different spatial resolutions. In this study, these seven networks were resampled at different spatial scales of small-scale (9/10 km), medium-scale (25 and 50 km) and large-scale (100 km) according to spatial grid resolution of remote sensing SSM products. The example diagram of four resampling scales (i.e. 9/10 km, 25 km, 50 km and 100 km) is shown in Figure 1. The ESA/CCI Level 4 global 2015 Land Cover map, with a spatial grid resolution of 300 m, was utilised to identify the land cover type of each in-situ SSM measurement site (http://www.esa-landcover-cci.org/). Overall, the primary land cover types among the 201 sites in the seven multi-scale observation networks were cropland, grassland, woodland, and shrubland.
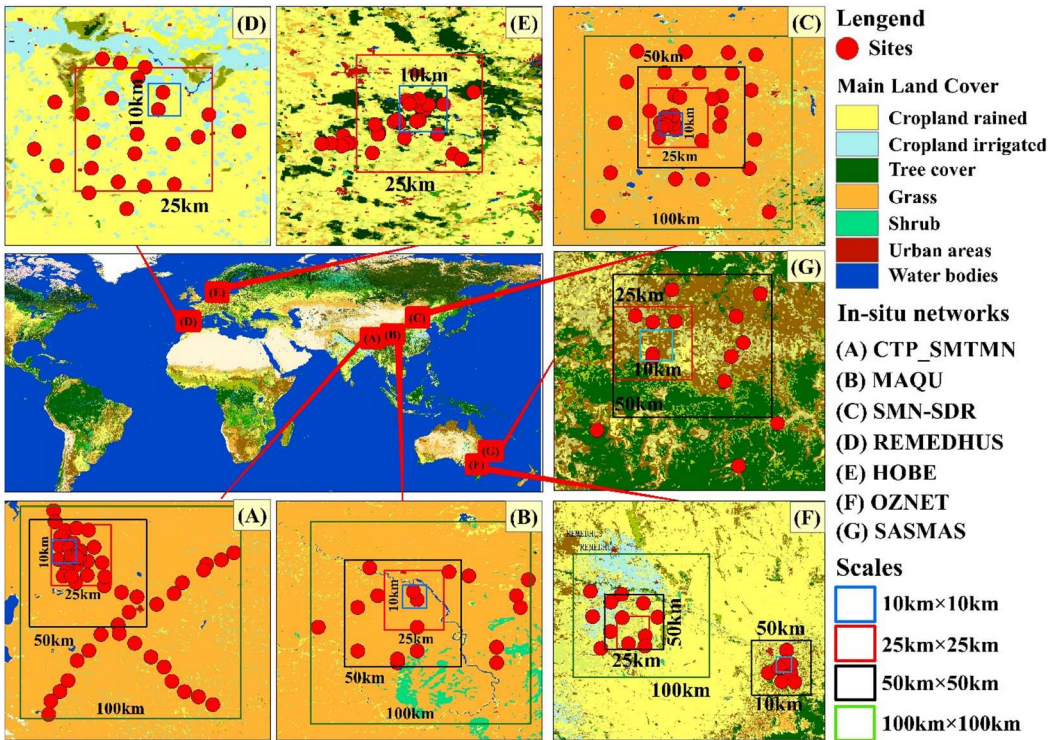
Figure 1. Spatial distribution of seven in-situ SSM measurement networks (CTP_SMTMN, MAQU, SMN-SDR, REMEDHUS, HOBE, OZNET and SASMAS) in land cover type map. The different colour box represents different sampling scales including 100 km (green), 50 km (black), 25 km (red) and 10 km (blue).

2.3. Dataset preprocessing

2.3.1. Preprocessing of global soil moisture products

In this study, for global-scale SMAP, ASCAT, ESA/CCI and GLDAS SSM products, three main pre-processing steps involving unit conversion, quality control, and resampling were applied.

Except for ASCAT and GLDAS products, the units of ESA/CCI and SMAP SSM products are Volumetric Soil Moisture (VSM) in cm³/cm³. To maintain consistent units, i.e. VSM in cm³/cm³, we converted the saturation (%) of ASCAT to volumetric soil water content (cm³/cm³) using the spatial grid resolution of 0.10-degree soil porosity data released by Earth Data Search, requiring prior resampling of the 1-degree soil porosity data to 0.10-degree to match the ASCAT SSM product (Saxton and Rawls 2006). Additionally, the GLDAS SSM product (SSM_{GLDAS}) was initially estimated in kg/m². To convert it to VSM (cm³/cm³), the Soil Bulk Density (SBK, cg/cm³) and a top soil layer depth (SD) were required, with the known SD of GLDAS SSM product being 2.0 cm. The resampled SBK data with spatial grid resolution of 0.25-degree from Soil-Grids5000 m 2.0 was used for unit conversion followed the equation: VSM = SSM_{GLDAS} / (SBK * SD) (Amini et al. 2023; Piles, Ballabrera-Poy, and Muñoz-Sabater 2019).

There were unreliable estimates, for instance, soil moisture estimations equal to or less than 0 cm³/cm³, in SMAP, ESA/CCI, and ASCAT SSM products. The purpose of quality control is to eliminate these unreliable SSM values from the global surface SSM product. Therefore, before assessing SMAP, ESA/CCI, and ASCAT SSM products, their quality control was executed using the quality flag values inherent to SMAP, ESA/CCI, and ASCAT SSM products themselves. For instance, in this study, SMAP-L2 data were masked out if the retrieval quality flag had a value other than 0 (Zheng et al. 2022). This approach was used to ensure that only the most reliable soil moisture

data were included in our analysis. Furthermore, there are inconsistencies in the SSM variation range between ASCAT, SMAP, ESA/CCI, and GLDAS products. Theoretically, soil moisture cannot be negative, and researches have shown there exists a saturation limit for soil moisture content i.e. 1.0 (cm³/cm³). If the SSM value of global surface SSM products exceeds 1.0 cm³/cm³, the retrieved SSM values were considered unreliable. In this study, negative SSM values and those exceeding 1.0 cm³/cm³ of SMAP, ASCAT, ESA/CCI and GLDAS SSM products were not considered.

To assess the accuracy of remote sensing SSM data products and systematically analyse potential mismatches with in-situ measurements, we applied resampling techniques on SMAP, ASCAT, ESA/CCI and GLDAS SSM products to four spatial scales (9/10 km, 25 km, 50 km, and 100 km). The primary motivation for this resampling was to standardise the comparison process across different datasets and spatial resolutions, enabling the effective identification and quantification of potential errors arising from differences in spatial resolution. By aligning all datasets to these common scales using an averaging pixel method, we were able to more accurately analyse the variability and discrepancies between in-situ SSM measurements and satellite-derived SSM products. Initially, we evaluated the original SMAP (9 km resolution), ASCAT (0.1° resolution), ESA/CCI and GLDAS (0.25° resolution) data at their native resolutions. Subsequently, a comprehensive analysis was conducted on the resampled original ESA/CCI and GLDAS data, with a spatial grid resolution of 0.25°, then we resampled SMAP, ASCAT, ESA/CCI and GLDAS SSM data products to ensure consistency and accuracy in the comparison.

2.3.2. Preprocessing of in-situ measurements

Regarding in-situ SSM measurement data, three primary preprocessing steps involved the removing abnormal values, site statistical analysis, spatial upscaling and temporal resampling. The in-situ SSM measurements used in this study were primarily taken at a soil depth of 0–5 cm to align with the depth sensitivity of the remote sensing SSM products. First, to maintain a consistent variation range of SSM with ASCAT, SMAP, ESA/CCI, and GLDAS products, abnormal values in in-situ soil moisture data (i.e. exceeding 1.0 cm³/cm³) were eliminated.

Secondly, when validating global-scale SSM products with coarse grid resolution using in-situ SSM measurement data, the quantity and distribution of in-situ stations within the same pixel directly impact the reliability of validation. Thus, this study tallied the pixel counts of SMAP, ASCAT, and ESA/CCI (or GLDAS) SSM products where stations of seven in-situ observation networks were situated (Figure 2A). Additionally, the study determined the maximum number of in-situ stations located in the same pixel of SMAP, ASCAT, and ESA/CCI (or GLDAS) SSM products (Figure 2B).

In Figure 2A, two scenarios are presented: 1) when only one in-situ station is available within the same pixel in the SMAP (ASCAT, ESA/CCI, GLDAS) SSM product; 2) when multiple in-situ stations (more than or equal to two) are present within the same pixel in the SMAP (ASCAT, ESA/CCI, GLDAS) SSM product. Observing Figure 2A, the pixel count (69 and 76) of SMAP and ASCAT respectively, with only one in-situ station, exceeds the count (31 and 42) of SMAP
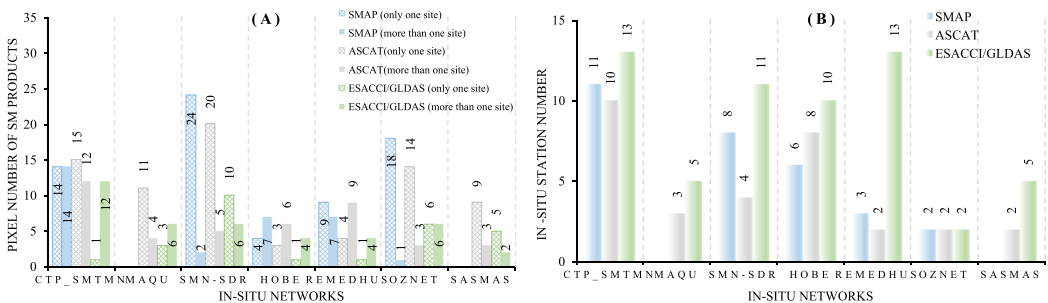

Figure 2. Pixel number histograms (A) and maximum of in-situ station number (B) of SMAP, ASCAT, ESA/CCI and GLDAS SSM products where in-situ stations are located.

Table 3. Maximum of in-situ observation sites located in the same ASCAT SSM grid at 10 , 25 , 50 and 100 km.

Resampling scales	In-situ observation networks						
	CTP_SMTMN	MAQU	SMN-SDR	HOBE	REMEDHUS	OZNET	SASMAS
10 km	10	3	4	8	2	2	2
25 km	21	4	9	21	10	4	5
50 km	29	12	12	26	12	5	12
100 km	29	15	19	26	12	9	12

and ASCAT within areas containing more than one in-situ station. Conversely, for ESA/CCI or GLDAS) (25 km) SSM products, the situation is reversed, with the pixel count (40) within areas containing more than one in-situ station exceeding the count (27) within areas with only one in-situ station. Figure 2B demonstrates that in the CTP_SMTMN network, the maximum number of in-situ stations located in the same pixel of SMAP, ASCAT, and ESA/CCI or GLDAS SSM product is higher compared to other in-situ observation networks, namely MAQU, SMN-SDR, REMEDHUS, HOBE, OZNET, and SASMAS.

Third, the in-situ SSM measurement data were also resampled into four spatial scales of 9/10 km, 25 km, 50 km, and 100 km using an upscaling method according to reference pixel grids of SMAP, ASCAT, ESA/CCI and GLDAS SSM product at spatial scales of 9/10 km, 25 km, 50 km, and 100 km. Using ASCAT SSM product as reference pixel grids, since the grid resolution of ASCAT SSM product was 10 km, resampling was necessary to match resolutions of 25 km, 50 km, and 100 km respectively. For each spatial grid resolution of ASCAT SSM product (10 km, 25 km, 50 km, and 100 km), pixels that contained the maximum in-situ observation sites within the same pixel were selected (refer to Table 3). The mean in-situ SSM values corresponding to these grids, which encompassed the most in-situ measurement sites, were computed at spatial scales of 10 km, 25 km, 50 km, and 100 km. The mean value of all in-situ SSM measurements within the same pixel of SMAP, ASCAT, ESA/CCI and GLDAS SSM products was considered as the 'true' SM value of that pixel.

The CTP_SMTMN and HOBE networks (Table 3) had more observation sites (i.e. 10, 21, 29, and 29 at 10 km, 25 km, 50 km, and 100 km respectively under CTP_SMTMN), surpassing other networks (MAQU, SMN-SDR, REMEDHUS, OZNET, and SASMAS). Additionally, the number of observation sites at the 100 km spatial scale exceeded that at 10 km. For example, under the SMN-SDR, there were 19 sites at 100 km spatial scale, but only 4 sites at 10 km. However, the average number of in-situ SSM observations per kilometre at 10 km spatial scale was notably higher than at 25 km, 50 km, and 100 km. For instance, within the CTP_SMTMN network, the average number of in-situ SSM observations at 10 km was 1 site per kilometre (10 sites/10 km), compared to 0.29 sites per kilometre (29 sites/100 km) at 100 km.

The temporal resolution of the in-situ measurement data is hourly. To align these with the global soil moisture products, different methods were employed to obtain the corresponding in-situ SSM data, rather than simply aggregating all the measurements into daily averages. For the SMAP product, which has overpass times at 06:00 and 18:00, the in-situ SM measurements at those exact times were directly used to match with the SMAP products. For the ASCAT product, with overpass times at 09:30 and 21:30, since these times do not align with full hours, we calculated the average of the in-situ measurements from 09:00–10:00 to represent the 09:30 value, and similarly, the average from 21:00–22:00 for the 21:30 value.

3. Methodology

3.1. Approach

In assessing remote sensing SSM data products with coarse grid resolution (≥9 km), it is imperative to validate them against in-situ measurements while accounting for any spatial coverage disparities. This study introduced a methodology to address footprint mismatches in evaluating remote sensing
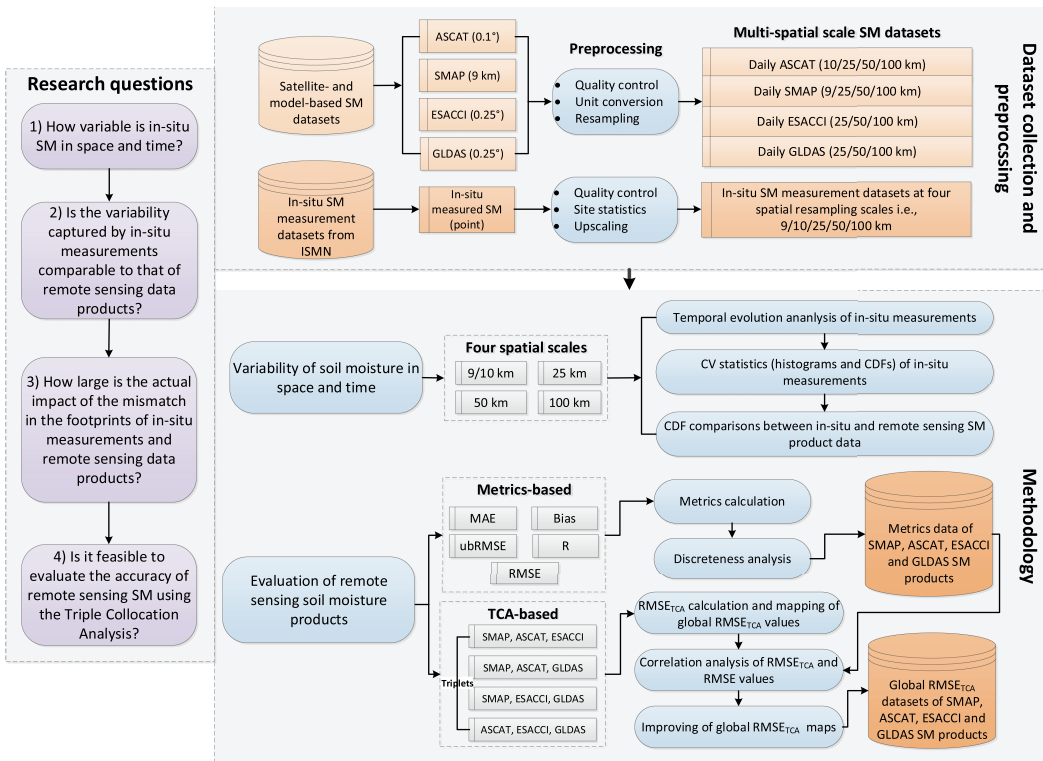
Figure 3. The evaluation approach of remote sensing soil moisture data products.

SSM data products (e.g. SMAP, ASCAT, ESA/CCI, and GLDAS), employing a comprehensive approach encompassing temporal evolution analysis, CV statistics, CDF comparison, error metrics, and the TCA method (Figure 3). Initially, to reveal how variable was in-situ SSM in space and time, the temporal evolution analysis and CV statistics were used based on in-situ SSM measurements sourced from seven observation networks (CTP_SMTMN, MAQU, SMN-SDR, REMEDHUS, HOBE, OZNET, and SASMAS) obtained from ISMN, across spatial scales ranging from 10 km to 100 km. Subsequently, to analyse whether the variability captured by in-situ measurements was comparable to that of remote sensing data products, CDF comparisons between remote sensing SSM products and in-situ measurements were conducted at varying spatial resolutions (9/10 km, 25 km, 50 km, and 100 km). The performance of SMAP, ASCAT, ESA/CCI, and GLDAS SSM products against in-situ data was evaluated using five error metrics: MAE, RMSE, ubRMSE, Bias, and R. This study compared error metric values at different spatial scales (9/10 km, 25 km, 50 km, and 100 km) to reveal the actual impact of the mismatch in the footprints of in-situ measurements and remote sensing data products. Finally, the study also employed the TCA method to estimate global-scale errors of these remote sensing SSM products. We explored the correlation between error values derived from the TCA-based algorithm and RMSE metric values from in-situ SSM measurements to reveal the feasibility of accuracy evaluation of remote sensing SSM using the TCA. For a deeper understanding, the following sections elaborate on each component of the methodology.

3.2. Temporal evolution and Coefficient of Variation of in-situ SSM

To reveal how variable was in-situ SSM in time, this study compared the spatio-temporal evolution of seven multi-scale in-situ SSM measurements (i.e. 9/10 km, 25 km, 50 km, and 100 km) to gain a

comprehensive understanding of spatiotemporal SSM variability. Among these, the multi-scale in-situ SSM measurements from seven observation networks (CTP_SMTMN, MAQU, SMN-SDR, HOBE, REMEDHUS, OZNET, and SASMAS) were generated using an upscaling method (Equation 1) matched with the pixel size (9 km of SMAP, 0.1° of ASCAT, and 0.25° of ESA/CCI and GLDAS) of global-scale SSM products:

$$\overline{SM_{in-situ}} = \frac{\sum_{i}^{W}\sum_{j}^{W}(SM_{in-situ})_{i,j}}{Count(SM_{in-situ})_{N \times N}} \tag{1}$$

where the W is the size of pixel i.e. 9/10 km, 25 km, 50 km and 100 km in this study; $\overline{SM_{in-situ}}$ is the averaging value of all in-situ SSM measurements within the $W \times W$ pixel window; the i and j represent the row and column indices of pixel in the $W \times W$ window, respectively; $(SM_{in-situ})_{i,j}$ is the in-situ SSM measurements in the indices of i row and j column; $Count(SM_{in-situ})_{N \times N}$ is the number of all in-situ SSM measurements within the $N \times N$ window.

To reveal how variable was in-situ SSM in space, we employed the Coefficient of Variation (CV). The CV index is a statistical measure employed to assess the extent of variability within datasets. It enables comparisons between variabilities of different datasets, even when their means and standard deviations differ. A higher value indicates higher data variability, while a lower value implies lower variability. Its significance lies in furnishing a standardised method for comparing the variabilities across various datasets. The formula for calculating the CV at each spatial scale entails dividing the standard deviation by the mean and then multiplying the result by 100% for representation as a percentage (Equation 2):

$$CV_{(j,t)} = \frac{\sigma\{SM_{(j,t)}\}}{mean\{SM_{(j,t)}\}} * 100\% \tag{2}$$

where the j represents the spatial scale (10 km, 25 km, 50 km and 100 km); $SM_{(j,t)}$ is the in-situ soil moisture value at spatial scale of j on t-th day; $\{SM_{(j,t)}\}$ represent a set of in-situ soil moisture of all sites at spatial scale of j on t-th day; $\sigma\{SM_{(j,t)}\}$ and $mean\{SM_{(j,t)}\}$ represent the standard deviation and average between the in-situ soil moisture values at 10 km, 25 km, 50 km and 100 km.

3.3. Cumulative distribution function

The CDF describes the probability distribution of a random variable. It possesses versatility, capable of modelling various types of random variables, whether continuous or discrete (Equation 3). It is calculated as:

$$F(x) = P(X \leq x), x = 0.1, \ 0.2, \ \ldots, 1.0 \tag{3}$$

where X represents the soil moisture value of in-situ SSM measurements or the pixel value of SMAP, ASCAT, ESA/CCI and GLDAS SSM products; x represents the SSM value at intervals of 0.1 cm³/cm³ from 0~1.0 cm³/cm³; $P(X \leq x)$ is the probabilities of all X values less than or equal to x. In this study, CDF calculations for SMAP, ASCAT, ESA/CCI and GLDAS SSM products required the spatial resampling of these products to match our designated spatial scales (9/10 km, 25 km, 50 km, and 100 km) of in-situ SSM measurements (Figure 1).

3.4. Evaluation metrics

In this study, five metrics (Equation 4~8) i.e. Mean Absolute Error (MAE, cm³/cm³), Root Mean Square Error (RMSE, cm³/cm³), Unbiased Root Mean Square Error (ubRMSE, cm³/cm³), Bias (cm³/cm³), and correlation coefficient (R) were employed to assess the global remote sensing

SMAP, ASCAT, ESA/CCI and GLDAS SSM products using in-situ SSM measurement data (Colliander et al. 2018; Zheng et al. 2022). Their calculation formulas are given by:

$$\text{MAE} = \sum_{i=1}^{N} (\text{SM}_i^E - \text{SM}_i^o)/N \tag{4}$$

$$\text{RMSE} = \sqrt{\sum_{i=1}^{N} (\text{SM}_i^E - \text{SM}_i^o)^2/N} \tag{5}$$

$$\text{ubRMSE} = \sqrt{\sum_{i=1}^{N} \left((\text{SM}_i^E - \overline{\text{SM}^E}) - (\text{SM}_i^o - \overline{\text{SM}^o})\right)^2/N} \tag{6}$$

$$\text{Bias} = |\overline{\text{SM}^E} - \overline{\text{SM}^o}| \tag{7}$$

$$\text{R} = \frac{\text{cov}(\text{SM}_i^E, \text{SM}_i^o)}{\sigma_{\text{SM}_i^E}\sigma_{\text{SM}_i^o}}, \quad \begin{cases} \text{cov: covariance} \\ \sigma\text{: standard deviation} \end{cases} \tag{8}$$

where SM_i^E (cm^3/cm^3) is the estimated SM value on ith day; $\overline{\text{SM}^E}$ (cm^3/cm^3) is the mean value of estimated SM value; SM_i^o (cm^3/cm^3) is the in-situ measured SM on ith day; $\overline{\text{SM}^o}$ is the mean value of in-situ measured SSM; N is the number of in-situ SSM measurements calculated by Equation 1.

3.5. Triple Collocation Analysis

The TCA method represents an error estimation approach that entirely eliminates reliance on in-situ measured data. Each soil moisture dataset within every pixel of remote sensing SSM data products can be represented as a linear relationship with the true SSM (Dorigo et al. 2010; McColl et al. 2014; Xie et al. 2022). The linear equation is given by:

$$\text{SM} = \alpha + \beta * t + \varepsilon \tag{9}$$

where SM (cm^3/cm^3) presents the SSM pixel value of SMAP, ASCAT, ESA/CCI or GLDAS products; ε is the random error; t (cm^3/cm^3) is the true SSM value; α and β are the coefficients. Then, the covariance equation (Q_{ij}) of any two remote sensing SSM data sets between SMAP, ASCAT, ESA/CCI and GLDAS SSM products is given by:

$$Q_{ij} = \beta_i\beta_j\sigma_t^2 + \beta_i\text{Cov}(t, \varepsilon_j) + \beta_j\text{Cov}(t, \varepsilon_i) + \text{Cov}(\varepsilon_i, \varepsilon_j) \tag{10}$$

where Q_{ij} is the covariance matrix of ith and jth remote sensing SSM data sets between SMAP, ASCAT, ESA/CCI and GLDAS SSM products; σ_t^2 is the variance of true SM value (t, cm^3/cm^3); $\text{Cov}(t, \varepsilon_j)$ the covariance matrix of jth remote sensing SSM data product with true SSM value; $\text{Cov}(t, \varepsilon_i)$ the covariance matrix of ith remote sensing SSM data product with true SSM value; β_i and β_j are the coefficients. The 3×3 covariance matrix of any three remote sensing SSM data sets between SMAP, ASCAT, ESA/CCI and GLDAS SSM products can be expressed as:

$$Q_{ij} = \begin{bmatrix} Q_{11} & Q_{12} & Q_{13} \\ Q_{21} & Q_{22} & Q_{23} \\ Q_{31} & Q_{32} & Q_{33} \end{bmatrix}, \quad \begin{cases} i = 1, 2, 3 \\ j = 1, 2, 3 \end{cases} \tag{11}$$

If the assumption that three SSM data sets are independent of each other is true, and when i is not equal to j in Equation 10, $\text{Cov}(\varepsilon_i, \varepsilon_j)$, $\text{Cov}(t, \varepsilon_i)$ and $\text{Cov}(t, \varepsilon_j)$ in Equation 10 are equal to zero. When i is equal to j in Equation 9, the $\text{Cov}(t, \varepsilon_j)$ and $\text{Cov}(t, \varepsilon_i)$ are equal to zero, but

$Cov(\varepsilon_i, \varepsilon_j)$ is not equal to zero. Then, Equation 10 will be simplified as:

$$Cov(SM_i, SM_j) = \begin{cases} \beta_i\beta_j\sigma_t^2, \ i \neq j \\ \beta_i\beta_j\sigma_t^2 + \sigma_{\varepsilon i}^2, \ i = j \end{cases}, \quad \begin{cases} i = 1, 2, 3 \\ j = 1, 2, 3 \end{cases} \tag{12}$$

From Equation 11, the 3×3 covariance matrix includes six unique terms i.e. Q_{11}, $Q_{12} = Q_{21}$, $Q_{13} = Q_{31}$, Q_{22}, $Q_{23} = Q_{32}$, Q_{33}. So, the six covariance equations can be obtained. However, in six covariance equations there are seven unknowns i.e. β_1, β_2, β_3, $\sigma_{\varepsilon 1}^2$, $\sigma_{\varepsilon 2}^2$, $\sigma_{\varepsilon 3}^2$, σ_t^2, which makes it impossible to obtain a unique solution. To obtain the unique solution, a new variable (θ_i) is introduced to Equation 12, and the θ_i is assumed to be equal to $\beta_i\sigma_t$. Then, Equation 12 can be rewritten as:

$$Cov(SM_i, SM_j) = \begin{cases} \theta_i\theta_j, i \neq j \\ \theta_i^2 + \sigma_{\varepsilon i}^2, i = j \end{cases}, \quad \begin{cases} i = 1, 2, 3 \\ j = 1, 2, 3 \end{cases} \tag{13}$$

From Equation 13, there are six equations (Q_{11}, $Q_{12} = Q_{21}$, $Q_{13} = Q_{31}$, Q_{22}, $Q_{23} = Q_{32}$, Q_{33}) and six unknowns (θ_1, θ_2, θ_3, $\sigma_{\varepsilon 1}^2$, $\sigma_{\varepsilon 2}^2$, $\sigma_{\varepsilon 3}^2$) to calculate the unique value for each unknown. Therefore, from Equation 11, the unique root-mean-square-error ($RMSE_{TCA}$) of each of SSM data set can be estimated as:

$$\begin{cases} RMSE_{TCA}^1 \\ RMSE_{TCA}^2 = \\ RMSE_{TCA}^3 \end{cases} \begin{bmatrix} \sqrt{Q_{11} - \dfrac{Q_{12}Q_{13}}{Q_{23}}} \\ \sqrt{Q_{22} - \dfrac{Q_{12}Q_{23}}{Q_{13}}} \\ \sqrt{Q_{33} - \dfrac{Q_{23}Q_{13}}{Q_{12}}} \end{bmatrix} \tag{14}$$

Due to the distinct SSM retrieval algorithms used in the SMAP, ASCAT, ESA/CCI and GLDAS SSM products, i.e. the SCA-V algorithm for SMAP, the TU-Wien for ASCAT, and the TCA-based merging algorithm for ESA/CCI, this study assumed independence among SMAP, ASCAT and ESA/CCI. However, in the ESA/CCI V7.1 product, both the SMAP and ASCAT SSM products have been merged into the ESA/CCI V6.1 product, despite the SMAP SSM product adopting the LPRM SSM retrieval algorithm, different from the SCA-V algorithm. This raised the possibility of errors in the ESA/CCI SSM product being linked to errors in the ASCAT and SMAP products, potentially violating the assumptions of the TCA method. To ensure a reliable evaluation of SMAP, ASCAT, and ESA/CCI using the TCA method, the GLDAS SSM product was added as the third dataset, replacing one of the SMAP, ASCAT, or ESA/CCI products in this study. Theoretically, the GLDAS SSM product, derived from the global land data assimilation system, can be considered a wholly independent product from SMAP, ASCAT, and ESA/CCI SSM products. Hence, in this study, a combination strategy involving SMAP, ASCAT, ESA/CCI, and GLDAS SSM products was proposed for the TCA method, as detailed in Table 4 (Triplet 1-4).

4. Results

4.1. Temporal evolution and spatial variability of in-situ soil moisture measurements

This study utilised in-situ SSM measurements collected from seven observation networks (CTP_SMTMN, MAQU, SMN-SDR, HOBE, REMEDHUS, OZNET, and SASMAS). These measurements were upscaled four resampling scales (10 km, 25 km, 50 km and 100 km) using the method described in Equation 1. The temporal variation and CV (Eq.2) index were employed to acess the spatial differences across these scale datasets. Figure 4 showed the temporal variation diagrams and CV statistics (histograms and CDFs) of in-situ SSM measurement data at four spatial scales (10 km, 25 km, 50 km and 100 km) according to reference grids of ASCAT SSM product at these four spatial scales (refer to Table 3).

Table 4. Combinations of SMAP, ASCAT, ESA/CCI and GLDAS SSM products used for TCA method.

	Triplets (SM_1, SM_2, SM_3)	Pairs for covariance		
		(SM_1, SM_2)	(SM_1, SM_3)	(SM_2, SM_3)
1	SMAP, ASCAT, ESA/CCI	SMAP, ASCAT	SMAP, ESA/CCI	ASCAT, ESA/CCI
2	SMAP, ASCAT, GLDAS	SMAP, ASCAT	SMAP, GLDAS	ASCAT, GLDAS
3	SMAP, ESA/CCI, GLDAS	SMAP, ESA/CCI	SMAP, GLDAS	ESA/CCI, GLDAS
4	ASCAT, ESA/CCI, GLDAS	ASCAT, ESA/CCI	ASCAT, GLDAS	ESA/CCI, GLDAS

Seasonal patterns: distinct seasonal variations were observed in CTP_SMTMN, SMN-SDR, and MAQU (Figure 4) networks, where SSM values peaked in August (summer) and were lowest in December (winter) each year. The maximum in-situ SSM measurement values varied across networks, reflecting regional differences in seasonal dynamics, with minimum values around 0.05 cm^3/cm^3, while maximum values reached approximately 0.4 cm^3/cm^3 (CTP_SMTMN), 0.5 cm^3/cm^3 (MAQU) and 0.3 cm^3/cm^3 (SMN-SDR), highlighting the substantial impact of resampling scales on in-situ SSM data.

Spatial variability: the results revealed considerable differences in in-situ SSM data across varying resampling scales, particularly in networks like REMEDHUS, where pronounced spatial heterogeneity was observed. For example, significant variations in CV values were noted, indicating that spatial resolution plays a crucial role in the interpretation of SSM data. Networks like HOBE, OZNET and SAS-MAS showed minimal seasonal variation and less pronounced differences across scales.

Quantitative disparities across resampling scales: the analysis of CV statistics (histograms and CDFs) further underscored the spatial heterogeneity in in-situ SSM data across resampling scales (10 km, 25 km, 50 km and 100 km). Striking differences in CV values were particularly evident in the CTP_SMTMN and REMEDHUS networks, with CVs reaching approximately 15.9% and 44% respectively. This suggests that upscaling in-situ SSM measurements from fewer sites such as two 10km-scale sites in REMEDHUS, may not accurately represent the broader spatial grid at that scale (see Table 3). Conversely, networks like HOBE displayed minimal differences in CV values across scales, with most values below 10%, while MAQU and SMN-SDR networks had mostly CV values below 20%. In contrast, CTP_SMTMN and SASMAS networks showed slightly asymmetric CV distribution, concentrated between 10% and 30%, and 20% and 40%, respectively.

Overall, the in-situ SSM data across different spatial scales effectively captured both intra – and inter-annual variability. This analysis underscores the importance of considering spatial scale when evaluating SSM dynamics, as subtle differences in temporal evolution across scales can provide insights into the dynamic characteristics of soil moisture over time. In addition, the CV index effectively captured the spatial differential characteristics of in-situ SSM measurements across varying scales, aiding in the assessment of the reliability of using these measurements to evaluate remote sensing SSM products such as ASCAT, SMAP, ESA/CCI and GLDAS.

4.2. CDF comparisons of in-situ and global-scale SSM data

To explore the relative performance of in-situ and global daily remote sensing SSM products (i.e. SMAP, ASCAT, ESA/CCI and GLDAS) across different spatial scales, we focused on comparing the shapes of the CDF (Equation 2) curves rather than their absolute values. CDF curves for in-situ, SMAP, ASCAT, ESA/CCI, and GLDAS SSM data from seven observation networks (i.e. CTP_SMTMN, MAQU, SMN-SDR, HOBE, REMEDHUS, OZNET and SASMAS) were compared across four spatial resampling scales: 10 km, 25 km, 50 km, and 100 km (Figure 5). To ensure valid comparisons, the temporal scales of in-situ measurements and remote sensing observations were aligned, including only data points where both datasets were available on the same days.

Comparison of CDFs Across Spatial Resampling Scales: when comparing the CDFs of in-situ SSM measurements across different spatial resampling scales (9/10 km, 25 km, 50 km, and 100 km)
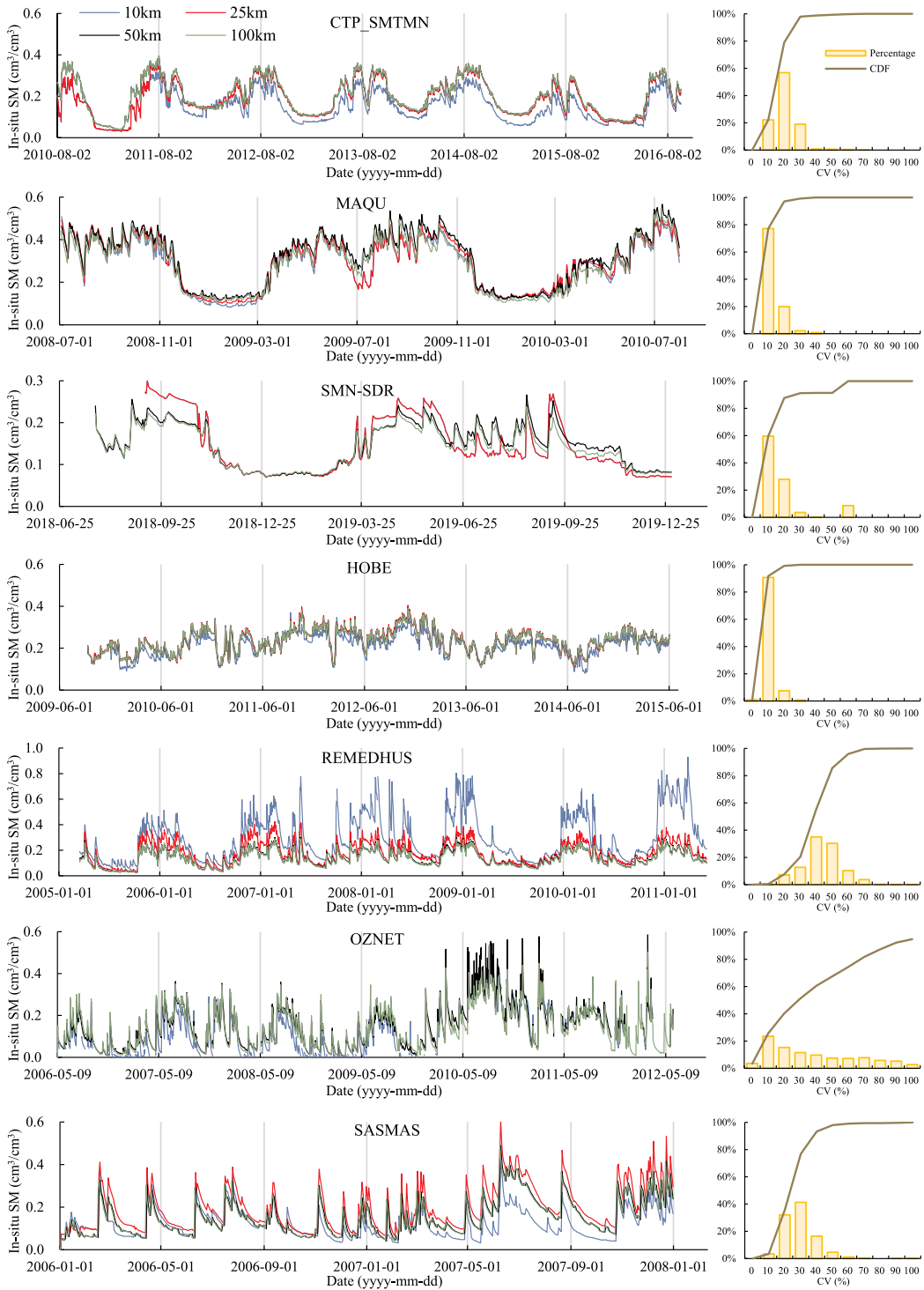
Figure 4. Temporal evolution and CV statistics (histograms and CDFs) of in-situ SSM measurements at CTP_SMTMN, MAQU, SMN-SDR, HOBE, REMEDHUS, OZNET and SASMAS observation networks at four spatial resampling scales of 10 km (blue), 25 km (red), 50 km (black) and 100 km (green).

within the same in-situ observation network, overall similarities in CDF shapes were noted, though subtle differences emerged. For instance, within the CTP_SMTMN network, in-situ SSM measurements around 0.3 cm³/cm³ exhibited nearly identical values across all four scales, with the slopes of the CDF curves being similar (0.0369, 0.0316, 0.0302, and 0.0302). Although the slopes of the CDF curves are similar across different spatial scales, there is a slight reduction in slope from 0.0369–0.0302 as the spatial scale increases, with the slopes at 50 km and 100 km being nearly identical. This slight decrease aligns with the time evolution patterns observed in the Figure 4, where variability tends to diminish at larger scales.

This finding applies to other networks such as MAQU, HOBE, REMEDHUS, OZNET, and SASMAS, particularly at the 25 km, 50 km, and 100 km scales, where the CDF were closely aligned. In the SMN-SDR network, CDFs at 10 km and 25 km scales shapes were similar shapes, as did those at 50 km and 100 km scales. Notably, distinct turning points were observed around the 0.2 cm³/cm³ mark at the 10 km and 25 km scales.

Comparison with Remote Sensing SSM Products: CDFs of remote sensing SSM products (SMAP, ASCAT, ESA/CCI, and GLDAS) across different spatial resampling scales (from 9/10 km to 100 km) generally exhibited consistent shapes within each network. For instance, within the CTP_SMTMN network, when SMAP pixel values were around 0.5 cm³/cm³, CDF values at all four scales approached 100%, with similar slopes across scales. This pattern was also observed for ASCAT, ESA/CCI and GLDAS products.

However, differences were noted between the CDFs of in-situ SSM measurements and remote sensing SSM products (SMAP, ASCAT, ESA/CCI and GLDAS) across spatial resampling scales. For example, in the CTP_SMTMN network, the CDFs of SMAP SSM product consistently fell below that of in-situ SSM measurements beyond 14% threshold, indicating a potential underestimation by the SMAP product at larger scales (25 km, 50 km and 100 km). Similarly, discrepancies were observed with ESA/CCI and GLDAS SSM products, particularly at lower SSM values (below 0.2 cm³/cm³), where their CDFs deviated from the in-situ SSM measurements, though they aligned more closely at higher values.

Among the networks studied, the SMAP CDFs at 10 km and 25 km scales closely matched those of in-situ SSM measurements in the SMN-SDR network, with similar trends observed in REMEDHUS. In contrast, ASCAT CDFs at 50 km and 100 km scales aligned more closely with in-situ SSM measurements in the HOBE and SASMAS networks. Notably, ESA/CCI product values at 25 km, 50 km and 100 km scales consistently showed higher SSM values compared to in-situ measurements at networks such as CTP_SMTMN, SMN-SDR, REMEDHUS and OZNET, particularly when SSM values were below 0.2 cm³/cm³.

Overall, the comparison of CDFs between in-situ SSM measurements and remote sensing products across various scales highlights the potential for improving the accuracy of SMAP, ASCAT, ESA/CCI and GLDAS products through better alignment with in-situ data, particularly at critical SSM thresholds.

4.3. Remote sensing soil moisture products vs. in-situ soil moisture measurements

4.3.1. Evaluation metrics

To quantitatively evaluate the global SMAP, ASCAT, ESA/CCI, and GLDAS SSM products, we utilised five metrics: MAE (Eq. 4), RMSE (Eq. 5), ubRMSE (Eq. 6), Bias (Eq. 7), and R (Eq. 8). These metrics were employed to assess the performance the SMAP, ASCAT, ESA/CCI and GLDAS SSM products against in-situ measured SSM data across seven multi-scale in-situ SSM observation networks (CTP_SMTMN, MAQU, SMN-SDR, HOBE, REMEDHUS, OZNET, and SASMAS) at four spatial scales i.e. 9/10 km, 25 km, 50 km and 100 km. These metrics' scores for SMAP, ASCAT, ESA/CCI and GLDAS SSM products were presented in Table 5 and Figure 6. Due to the absence of SMAP SSM product data within the MAQU and SASMAS networks, the comparison was limited to the CTP_SMTMN, SMN-SDR, HOBE, REMEDHUS and OZNET networks in Table 5.
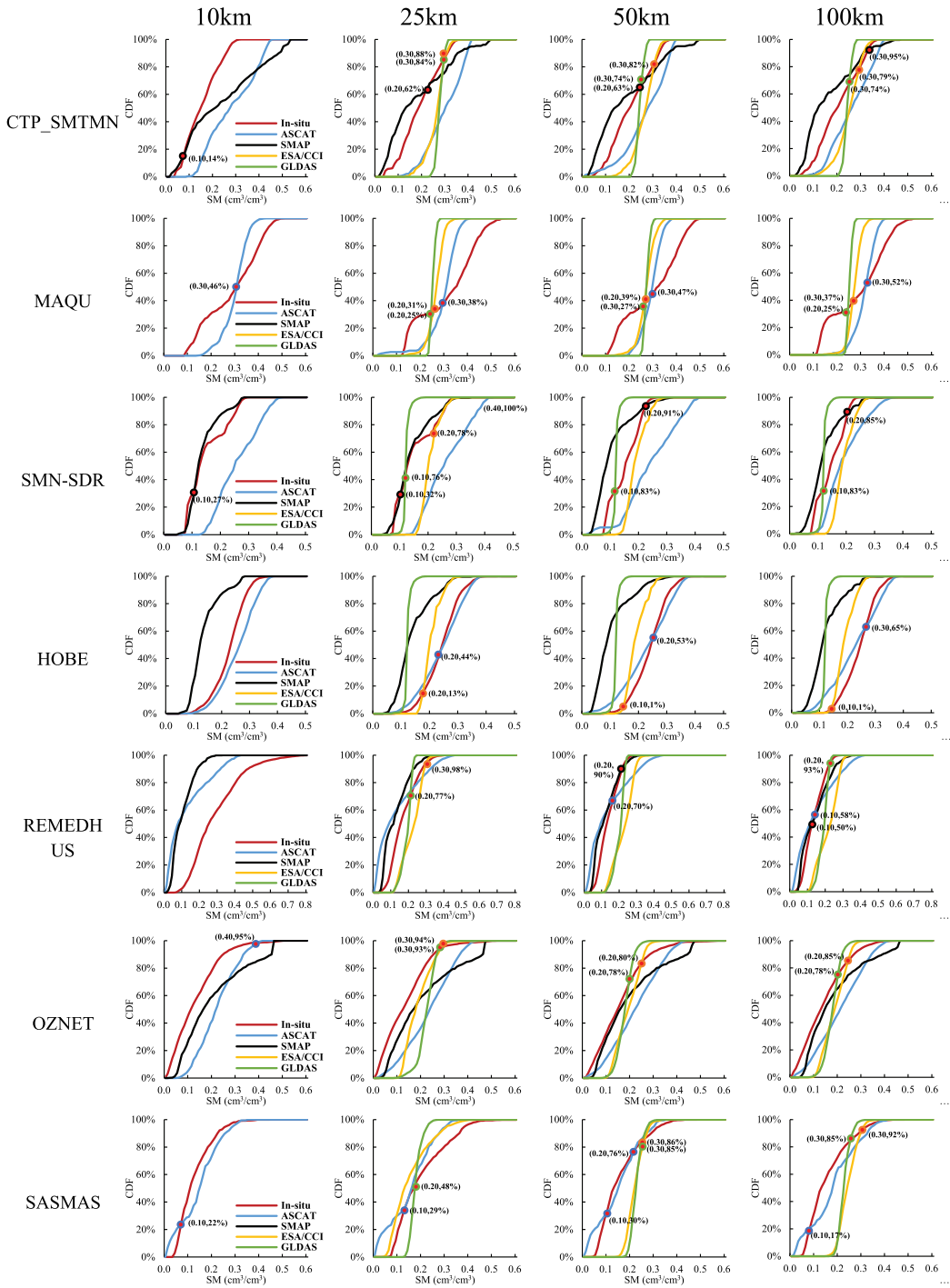
Figure 5. CDF comparisons of in-situ SSM measurement data (CTP_SMTMN, MAQU, SMN-SDR, HOBE, REMEDHUS, OZNET and SASMAS), SMAP, ASCAT, ESA/CCI and GLDAS SSM products under four spatial resampling scales (10 , 25 , 50 and 100 km).

Analysis of the metrics at 25 km, 50 km, and 100 km scales in Table 5 showed that SMAP and ESA CCI products generally correspond better with in-situ data compared to ASCAT and GLDAS, as evidenced by their lower ubRMSE, MAE, RMSE and Bias values, and higher R values. This

finding is consistent with the study by Beck et al. 2021 (e.g. https://doi.org/10.5194/hess-25-17-2021) (Beck et al. 2021). In addition, an interesting trend emerged: as the spatial scale increased from 9 km to 100 km, the MAE and RMSE values for SMAP decreased while R values increased, particularly in the OZNET network. However, this trend did not hold for ubRMSE and Bias values, which may indicate a bias-variance trade-off at play, where larger scales reduce variance but potentially introduce bias due to increased averaging effects. For instance, within the CTP_SMTMN network, SMAP's MAE and RMSE values at 100 km (0.051 cm^3/cm^3 and 0.059 cm^3/cm^3) were lower than those at 10 km (0.068 cm^3/cm^3 and 0.080 cm^3/cm^3), with the R value at 100 km (0.904) higher that at 10 km (0.869). ASCAT displayed a similar pattern. For example, in the SMN-SDR network, the MAE at 100 km was almost half that at 10 km (0.059 cm^3/cm^3 and 0.109 cm^3/cm^3), indicating the greater impact of mismatches between the footprints of in-situ measurements and SMAP/ASCAT data at smaller scales.

Conversely, ESA/CCI and GLDAS products often exhibited the opposite trend. For instance, in CTP_SMTMN network, the RMSE value for ESA/CCI product at 25 km (0.033 cm^3/cm^3) was lower than at 100 km (0.043 cm^3/cm^3), and the R value at 25 km (0.813) exceeded that at 100 km (0.792). Similarly, GLDAS had a lower MAE at 100 km (0.073 cm^3/cm^3) than at 25 km (0.098 cm^3/cm^3). The mismatch between in-situ measurements and ESA/CCI or GLDAS products was less significant compared to SMAP and ASCAT. For instance, in the SMN-SDR network, the difference in MAE values for ESA/CCI product between 100 km and 25 km scales was 0.007 cm^3/cm^3, while GLDAS showed a smaller difference of 0.01 cm^3/cm^3.

In summary, SMAP product showed higher consistency with in-situ SM measurements at larger scales (e. g., 100 km) compared to smaller spatial scales (e.g. 9 km/10 km). Conversely, ESA/CCI product showed better consistency at smaller scales (e.g.25 km). An inverse trend was observed for SMAP and ASCAT products, with the impact of mismatches being more pronounced as smaller scales, while ESA/CCI and GLDAS showed opposite trend.

4.3.2. Box-plots of all metrics values

In this study, we compared the all-metrics of SMAP, ASCAT, ESA/CCI and GLDAS SSM products at spatial resampling scales of 9/10 km, 25 km, 50 km, and 100 km, using in-situ SSM measurements gathered from seven observation networks (CTP_SMTMN, MAQU, SMN-SDR, HOBE, REMED-HUS, OZNET, and SASMAS). The results, presented in box-plots (Figure 6) revealed several key patterns.

When comparing metrics across different scales, SMAP consistently exhibited lower MAE, RMSE and Bias values, particularly at larger spatial scales (50 km and 100 km), indicating a higher consistency with in-situ SSM measurements. For example, SMAP showed a more stable performance, with lower variation in RMSE values at the spatial scale increased from 9 km to 100 km. This suggests that SMAP's accuracy improved with larger spatial scales, making is more reliable at these resolutions.

At a spatial scale of 9/10 km, SMAP product outperformed ASCAT in terms of MAE values, with showing lower maximum, minimum and average values (0.22 cm^3/cm^3, 0.03 cm^3/cm^3, and 0.07 cm^3/cm^3). At 25 km scale, although the differences between SMAP, ASCAT, ESA/CCI and GLDAS were less pronounced, SMAP still demonstrated superior performance with lowest maximum values for MAE, RMSE and Bias (0.15 cm^3/cm^3, 0.16 cm^3/cm^3, and 0.11 cm^3/cm^3), and the highest R values (0.93).

For ESA/CCI and GLDAS products, a clear trend emerged as the spatial scale increase from 25 km to 100km: the dispersion of MAE (or RMSE/ubRMSE/Bias/R) values decrease, suggesting a reduction in the impact of footprint mismatch. Notably, ASCAT showed the smallest variation in RMSE at 100 km scale compared to smaller scales, further indicating that larger scales mitigate the mismatch between in-situ measurements and remote sensing SSM products.

Overall, a consistent pattern was observed across SMAP, ASCAT, ESA/CCI, and GLDAS SSM products: the dispersion of metric values was lower at 100 km than smaller scales, implying reduced

Table 5. MAE (cm³/cm³), RMSE (cm³/cm³), Bias (cm³/cm³), ubRMSE(cm³/cm³) and R values of SMAP, ASCAT, ESA/CCI and GLDAS SSM products against in-situ SSM measurements at CTP_SMTMN, MAQU, SMN-SDR, HOBE, REMEDHUS, OZNET and SASMAS observation networks from ISMN (Metrics values of MAE, RMSE, and ubRMSE below 0.06 cm³/cm³, Bias less than 0.03 cm³/cm³, and R values exceeding 0.8 were highlighted in bold).

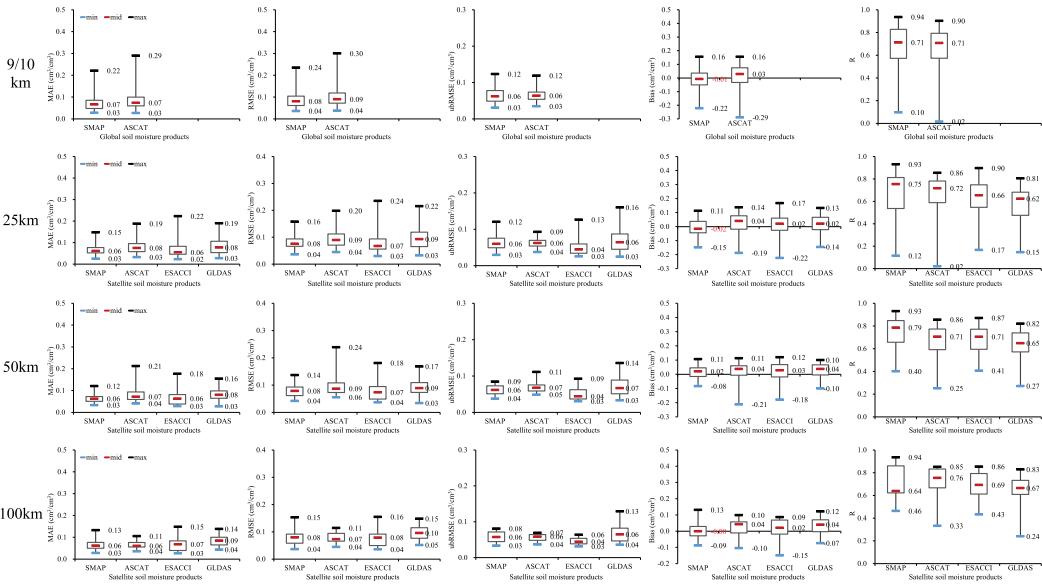| Metrics	Ob. networks	SMAP				ASCAT				ESA/CCI			GLDAS		
		9km	25km	50km	100km	10km	25km	50km	100km	25km	50km	100km	25km	50km	100km
MAE	CTP_SMTMN	0.068	0.066	0.068	**0.051**	0.092	**0.055**	**0.041**	**0.036**	**0.024**	**0.030**	**0.035**	0.098	0.082	0.073
	SMN-SDR	**0.057**	**0.053**	**0.050**	**0.049**	0.109	0.086	0.094	0.059	**0.024**	**0.029**	**0.031**	0.107	0.118	0.106
	HOBE	**0.050**	**0.048**	**0.038**	0.062	**0.047**	**0.049**	**0.054**	**0.052**	0.035	0.033	0.038	**0.045**	**0.043**	**0.044**
	REMEDHUS	0.067	**0.034**	**0.034**	**0.035**	0.071	0.073	0.067	**0.056**	0.074	0.092	0.085	**0.042**	0.060	0.086
	OZNET	0.080	0.088	0.069	0.062	0.083	0.102	0.077	0.078	0.097	0.066	0.066	**0.055**	0.066	**0.058**
RMSE	CTP_SMTMN	0.080	0.079	0.079	**0.059**	0.108	0.066	**0.056**	**0.045**	**0.033**	**0.037**	**0.043**	0.118	0.100	0.086
	SMN-SDR	0.068	0.063	**0.060**	**0.058**	0.127	0.105	0.113	0.071	**0.032**	**0.038**	0.039	0.117	0.129	0.117
	HOBE	0.062	0.062	**0.051**	0.089	0.057	0.062	0.069	0.065	**0.044**	**0.042**	0.047	**0.051**	**0.050**	**0.052**
	REMEDHUS	0.076	**0.045**	**0.042**	**0.046**	0.089	0.088	0.082	0.070	0.083	0.097	0.090	**0.054**	0.072	0.097
	OZNET	0.102	0.112	0.088	0.079	0.095	0.115	0.095	0.097	0.103	0.080	0.079	0.065	0.073	0.066
ubRMSE	CTP_SMTMN	0.078	0.078	0.078	**0.055**	0.061	**0.044**	**0.056**	**0.045**	**0.031**	**0.031**	**0.038**	0.071	0.075	0.075
	SMN-SDR	**0.053**	**0.055**	**0.053**	**0.046**	0.070	0.071	0.078	0.061	**0.030**	**0.031**	0.032	0.111	0.116	0.111
	HOBE	0.061	**0.058**	**0.051**	0.081	**0.054**	0.062	0.068	0.064	**0.041**	**0.041**	**0.044**	**0.045**	**0.044**	**0.045**
	REMEDHUS	**0.044**	**0.044**	**0.040**	**0.044**	0.089	0.084	0.081	0.070	**0.044**	**0.033**	**0.031**	**0.044**	**0.044**	**0.047**
	OZNET	0.087	0.091	0.082	0.076	0.065	0.066	0.075	0.068	0.063	0.068	0.060	**0.049**	**0.036**	**0.036**
Bias	CTP_SMTMN	**0.015**	**0.008**	**0.016**	**0.022**	0.089	0.050	**0.001**	**0.005**	**0.011**	**0.020**	**0.021**	0.094	0.066	0.041
	SMN-SDR	0.043	0.031	**0.028**	0.035	0.106	0.078	0.082	0.037	**0.012**	**0.022**	**0.022**	0.037	0.056	0.039
	HOBE	**0.008**	**0.024**	**0.003**	0.037	**0.018**	**0.002**	**0.013**	**0.011**	**0.014**	**0.008**	**0.018**	**0.024**	**0.023**	**0.026**
	REMEDHUS	0.062	**0.010**	**0.015**	**0.014**	**0.006**	**0.026**	**0.005**	**0.006**	0.071	0.092	0.085	0.031	0.057	0.085
	OZNET	0.052	0.065	0.034	**0.022**	0.070	0.094	0.058	0.068	0.082	0.042	0.052	0.043	0.064	0.055
R	CTP_SMTMN	**0.869**	**0.891**	**0.886**	**0.904**	**0.880**	**0.826**	**0.820**	**0.848**	**0.813**	**0.812**	0.792	0.716	0.739	0.725
	SMN-SDR	0.480	0.409	0.402	0.464	0.385	0.424	0.509	0.333	0.556	0.518	0.482	0.601	0.672	0.653
	HOBE	0.576	0.628	0.701	0.625	0.598	0.571	0.594	0.645	0.718	0.626	0.651	0.296	0.281	0.241
	REMEDHUS	0.731	0.755	**0.802**	**0.860**	0.705	0.663	0.745	**0.823**	0.792	**0.841**	**0.855**	0.555	0.534	0.563
	OZNET	0.768	0.760	**0.811**	**0.820**	0.769	0.781	0.734	0.756	**0.843**	0.761	0.794	0.784	**0.822**	**0.820**

Figure 6. Box-plots of metrics values (MAE, RMSE, ubRMSE, Bias and R) of SMAP, ASCAT, ESA/CCI and GLDAS SSM products versus in-situ SSM measurements at CTP_SMTMN, MAQU, SMN-SDR, HOBE, REMEDHUS, OZNET and SASMAS observation networks from ISMN.

mismatches between in-situ and remote sensing product at larger scales. SMAP product consistently outperformed ASCAT, ESA/CCI, and GLDAS products at most scales from the box-plots of RMSE values, particularly at 25 and 50 km. However, at 100 km scale, ASCAT product showed better performance than SMAP, ESA/CCI, and GLDAS products.

4.4. Global-scale evaluation of Triple Collocation Analysis

4.4.1. Global-scale error estimation

To evaluate SMAP, ASCAT, ESA/CCI and GLDAS SSM data products in global-scale, this study used the TCA method based on the designated four triplets (see Table 4) to computed the $RMSE_{TCA}$ values. Figure 7 illustrates three global $RMSE_{TCA}$ maps for each SMAP, ASCAT, ESA/CCI, and GLDAS SSM product at a spatial grid resolution of 25 km, generated from Triplet 1–4.

From Figure 7, it was evident that the spatial distribution patterns were highly similar, with $RMSE_{TCA}$ values lower than 0.05 cm^3/cm^3 across most areas, especially in Northern Africa and Asia. Notably, the missing $RMSE_{TCA}$ values of SMAP SSM product were fewer in Triplet 2 compared to Triplet 1 and 3, potentially due to fewer missing values in ASCAT and GLDAS SSM products. Moreover, for ESA/CCI SSM product, the overall $RMSE_{TCA}$ values from Triplet 4 were lower than those from Triplet 1 and 3. In Triplet 1's $RMSE_{TCA}$ map of ESA/CCI SSM product, there was a distinct region with very high $RMSE_{TCA}$ values, surpassing 0.22 cm^3/cm^3, which was observed in the Qinghai-Tibet Plateau. Regarding the three global $RMSE_{TCA}$ maps of ASCAT SSM product from Triplet 1, 2, and 4, the Northern regions of North America and Asia exhibited notably high $RMSE_{TCA}$ values, almost exceeding 0.22 cm^3/cm^3. While the $RMSE_{TCA}$ values of GLDAS SSM product from Triplet 2–4 were also high in these Northern regions, those from Triplet 3 were lower compared to Triplet 2 and 4.

Additionally, to compare the spatial differences between the $RMSE_{TCA}$ of Triplet 1~4, we compiled and compared the histograms and CDFs of global $RMSE_{TCA}$ maps of SMAP, ASCAT, ESA/CCI, and GLDAS SSM products from Triplet 1–4, as depicted in Figure 8.
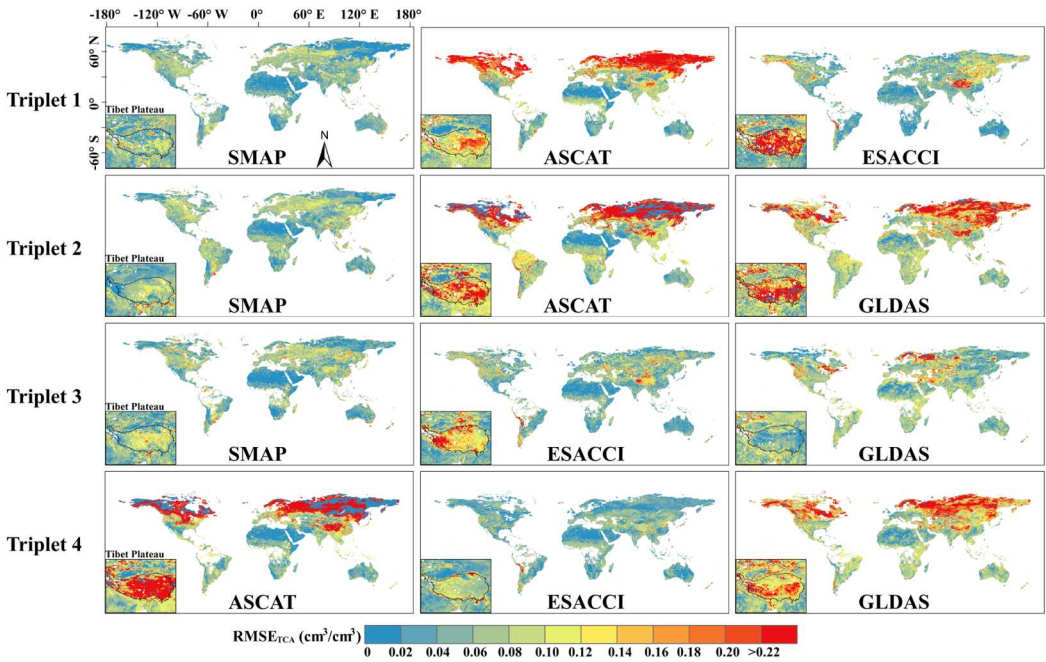
Figure 7. Global RMSE$_{TCA}$ maps of SMAP, ASCAT, ESA/CCI and GLDAS SSM products under 25 km of spatial scale.
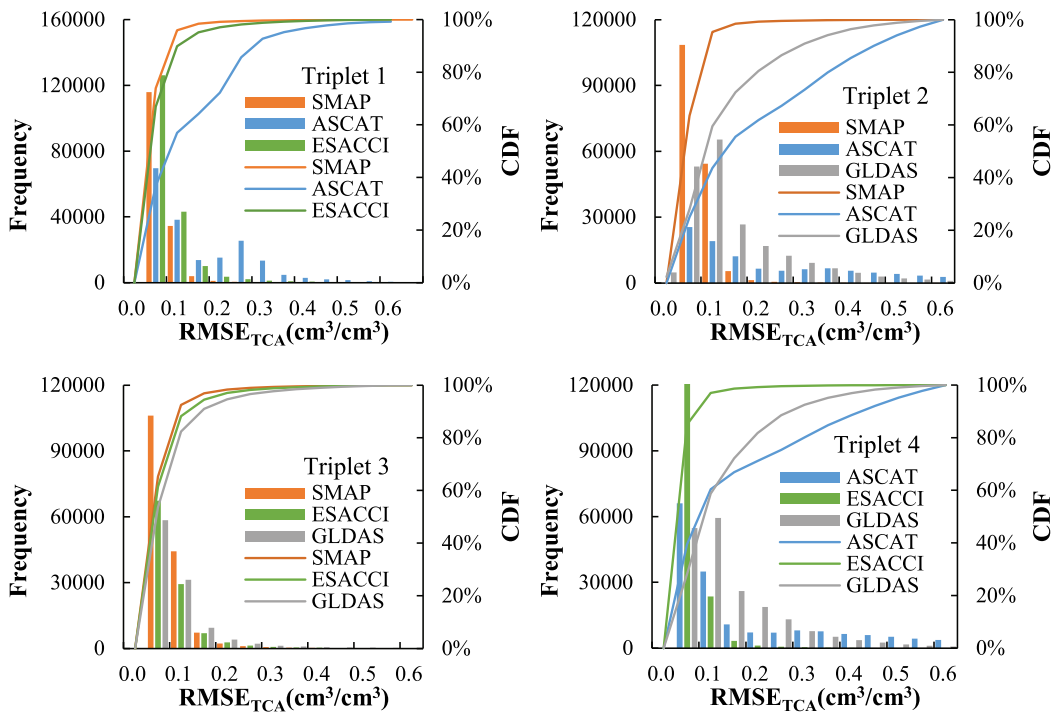

Figure 8. The histograms and CDFs of RMSE$_{TCA}$ values of SMAP, ASCAT, ESA/CCI and GLDAS SSM products under 25 km of spatial scale from Triplet 1–4.

The histograms of RMSE$_{TCA}$ values for SMAP, ASCAT, ESA/CCI, and GLDAS SSM products from Triplet 1–4 reveal significant variations across the different combinations. In Triplet 1, RMSE$_{TCA}$ values below 0.05 cm^3/cm^3 were more frequently observed in SMAP (74%), ASCAT (37%) and ESA/CCI (67%), indicating better performance of SMAP in this combination. Conversely, in Triplet 4, ESA/CCI exhibited the highest frequency of RMSE$_{TCA}$ values below 0.05 cm^3/cm^3 (85%), outperforming ASCAT (40%) and GLDAS (28%) products. Overall, the lower global RMSE$_{TCA}$ values of the SMAP SSM product across all triplets suggest that the SMAP SSM product consistently demonstrates better performance relatively ASCAT, ESA/CCI, and GLDAS products. This pattern indicates that the choice of product combinations significantly influences the evaluation outcomes using the TCA method. These results highlight the importance of selecting appropriate product combinations in multi-sensor soil moisture assessments and suggest that SMAP may offer more reliable estimates in diverse global conditions.

4.4.2. Comparisons with the errors of metrics-based algorithm

To analyse the feasibility of TCA method for evaluation accuracy of remote sensing SSM products, this study attempted to seek the relevance by the comparing of RMSE$_{TCA}$ values derived from the TCA-based algorithm with RMSE values calculated using in-situ measured SSM data. From the RMSE$_{TCA}$ maps (Figure 7) of SMAP, ASCAT, ESA/CCI, and GLDAS SSM products, the RMSE$_{TCA}$ values corresponding to in-situ measurement stations were isolated and analysed for correlation with RMSE values (using in-situ measured SM data) via scatter plot (Figure 9).

When comparing the RMSE$_{TCA}$ values of SMAP SM products with RMSE values directly calculated from in-situ measurements, distinct patterns of systematic biases within the datasets become apparent. Direct RMSE values measured against in-situ measurements provide an assessment of the absolute accuracy of a dataset, reflecting its real-world performance by including all error sources relative to ground measurements. In contrast, RMSE values derived from the TCA method evaluate the relative accuracy of a dataset within a triplet, separating random errors from systematic biases common across all datasets involved in the TCA. Therefore, by contrasting the RMSE derived from TCA with the direct RMSE from in-situ data, we can identify systematic biases present in the datasets.

In Triplet 1, the SMAP product's sample points were closely aligned with the 1:1 line, indicating a strong linear correlation between the RMSE$_{TCA}$ and RMSE values, with a correlation coefficient of 0.674, 0.190 and 0.472. This indicates that the RMSE$_{TCA}$ values from Triplet 1 may be more consistent with RMSE values obtained from in-situ measurements. A linear relationship (i.e. y = 0.805*x-0.05, where x represents RMSE and y represents RMSE$_{TCA}$) could potentially be used to correct the RMSE$_{TCA}$ maps of the SMAP product, leading to improved evaluation accuracy.

Similarly, in Triplet 2, ASCAT product showed a higher correlation (0.526) between RMSE$_{TCA}$ and RMSE values compared to SMAP and GLDAS products, suggesting that ASCAT's TCA-derived accuracy may be more reliable in this configuration. In Triplet 3, although the ESA/CCI product showed a concentrated alignment around the 1:1 line, GLDAS product exhibited a stronger correlation (R = 0.666) with in-situ RMSE values, despite GLDAS's RMSE$_{TCA}$ values consistently underestimating RMSE. However, in Triplet 4, no significant relationship between RMSE$_{TCA}$ and RMSE values was observed for ASCAT, ESA/CCI, or GLDAS SSM products, highlighting the variability in TCA's reliability depending on the triplet configuration.

In summary, the RMSE$_{TCA}$ values of SMAP in Triplet 1, ASCAT in Triplet 2, and ESA/CCI and GLDAS in Triplet 3 exhibited the correlations with RMSE values derived from in-situ measurements. These relationships could potentially be used to adjust the global RMSE$_{TCA}$ maps for these SSM products, thereby enhancing the reliability of their evaluations. Furthermore, it is important to note that the accuracy assessment of the same SSM product varied significantly provide reliable accuracy evaluations for remote sensing SSM products.
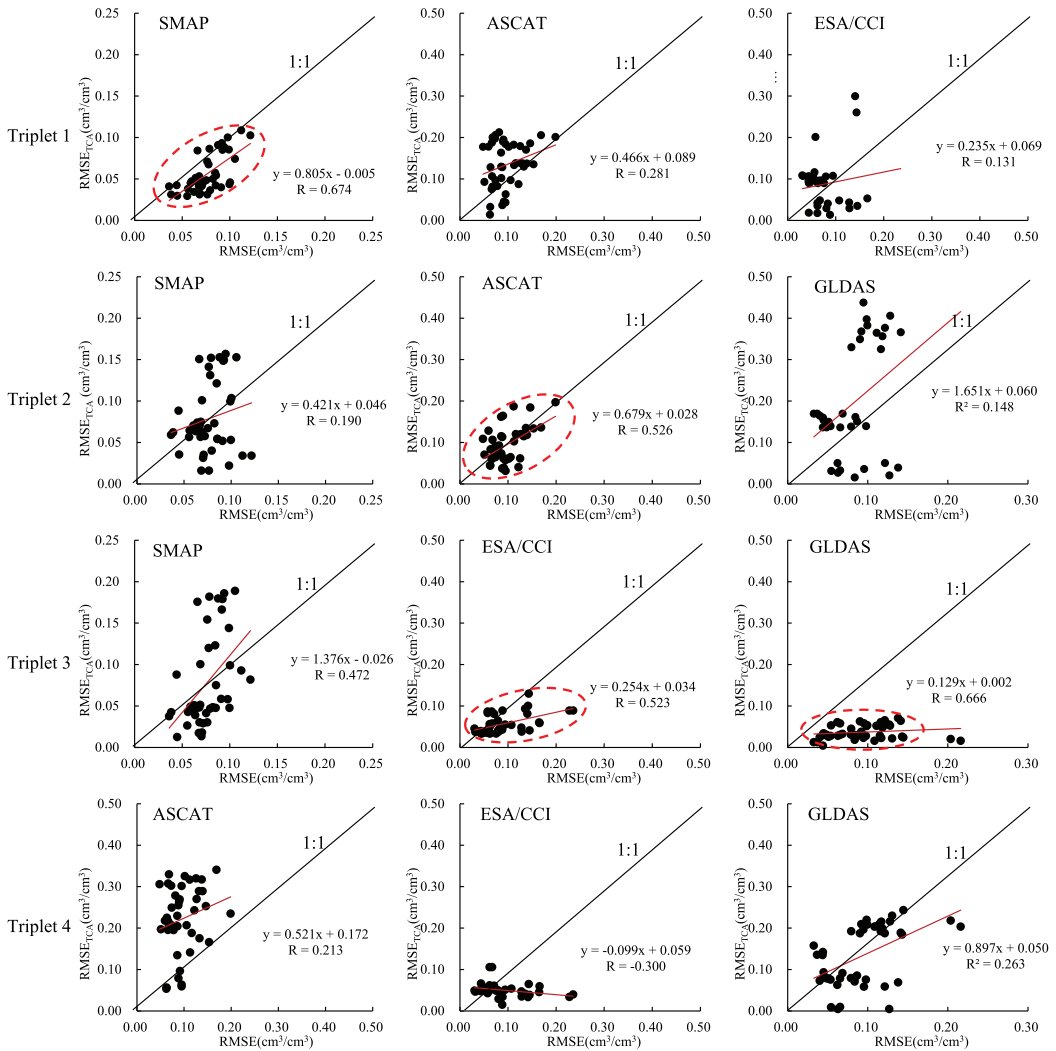
Figure 9. Scatter plots of RMSE$_{TCA}$ (using TCA algorithm from Triplet 1–4) and RMSE (using in-situ SSM measurement data) values of SMAP, ASCAT, ESA/CCI and GLDAS at 25 km spatial scale.

5. Discussion

5.1. Drivers of spatiotemporal variability in surface soil moisture

Our study revealed significant spatial variability in SSM across different spatial scales (i.e. 10 , 25 , 50 and 100 km) in networks such as CTP_SMTMN, REMEDHUS, and SASMAS. The CV values indicated that at finer scales (10 km), the SSM measurements were more consistent, while at across coarser scales (25 km, 50 km and 100 km), the variability increased markedly, with more than 70% of CV values exceeding 0.2, 0.3 and 0.2, respectively. This pattern can be the increased heterogeneity in soil properties and land cover as the spatial scale enlarges, where larger areas encompass more diverse environment conditions (Brocca et al. 2010; Wen et al. 2023; Zhao et al. 2014). In contrast, networks like MAQU, SMN-SDR and HOBE exhibited lower CV values across scales, suggesting minimal differences in SSM measurements at these sites. The strong temporal variability observed in the CV values further underscores the influence of dynamic environmental factors such as precipitation, temperature and land management practices on soil moisture levels (Mahmood

et al. 2012; Saeedi et al. 2023). For instance, rapid fluctuations in SSM observed in HOBE, OZNET and SASMAS networks could be linked to agricultural activities and varying precipitation patterns, highlighting the role of human intervention and climatic variability in modulating soil moisture (González-Zamora et al. 2015; Jensen and Illangasekare 2011; Meng et al. 2022; Seneviratne et al. 2010). The HOBE, OZNET and SASMAS in-situ observations suggest that irrigation water may be applied in these areas. The GLDAS model does not account for irrigation volumes, whereas satellite data may reflect the total water input, including irrigation. Therefore, the SSM simulated by GLDAS could be lower than the SSM observed by satellites. We did notice that in irrigated areas at times the GLDAS SSM is slightly lower than the SSM retrieved from satellite data, but not systematically. Based on the water balance calculation, if irrigation is not considered, the SSM from GLDAS should naturally be lower.

Furthermore, the seasonal variability in SSM was particularly evident in networks such as CTP_SMTMN and MAQU, where SSM levels were significantly lower from January to March (less than 0.1 cm^3/cm^3), and higher from July to September (more than 0.35 cm^3/cm^3). The seasonal trend reflects the strong influence of temperature and precipitation cycles on soil moisture dynamics (Mahmood et al. 2012). The differences in SSM variability across spatial scales, as capture in the temporal evolution plots, provide crucial insights into the scale-dependent nature of SSM dynamics. Understanding these mechanisms is essential for accurate assessment and interpretation of SSM data, especially when using in-situ measurements to validate remote sensing SSM products (Venegas-Cordero et al. 2023).

5.2. Performance of remote sensing SSM products across different spatial scales

ESA/CCI SSM product demonstrated superior accuracy at finer spatial scales, as evidenced by the lowest MAE, RMSE, and ubRMSE values (0.024 cm^3/cm^3, 0.032 cm^3/cm^3, and 0.030 cm^3/cm^3, respectively) observed at the 25 km scale within the SMN-SDR network. On the other hand, the ASCAT SSM product showed the lowest Bias value (0.001 cm^3/cm^3) at the 50 km spatial scale within the same network was, indicating minimal systematic error at this resolution. Notably, the SMAP SSM product achieved the highest correlation with in-situ measurements (R = 0.904) at the 100 km spatial scale within the CTP_SMTMN network, suggesting that SMAP is particularly well-suited for applications requiring coarser spatial resolution. These findings highlight the variability in the performance of different remote sensing SSM products depending on the spatial scale and the specific error metrics employed. (Skøien, Blöschl, and Western 2003; Wen et al. 2023). For instance, while SMAP and ASCAT SSM products exhibited the lower MAE and RMSE values and the higher correlation coefficients at larger spatial scales (e.g. 100 km), the ESA/CCI and GLDAS SSM products performed optimally at 25 km spatial scales, where they achieved lower RMSE and higher R values. This variation complicates efforts to rank remote sensing SSM products solely based on their accuracy, as the best-performing product can vary depending on both the spatial scale and the chose evaluation metric (Wen et al. 2023; Zhao et al. 2014). Given this complexity, it is essential to adopt a multifaceted evaluation approach that considers the specific requirements of the intended application and the spatial scale of interest. Such an approach ensures that the selected remote sensing SSM product is best aligned with the precision needs of the observational network and the intended use case.

Additionally, it was observed that SMAP and ASCAT SSM products demonstrated better consistency with in-situ SSM measurements at larger spatial scales (25 km, 50 km and 100 km), whereas ESA/CCI and GLDAS products exhibited less variability across different spatial scales. This may be attributed to reduced impact of vegetation and roughness on satellite-based SSM inversion as spatial resolution increases, leading to more stable retrievals at coarser scales (Xie et al. 2021). Overall, the reduced dispersion of metric values, such as MAE, observed for SMAP, ASCAT, ESA/CCI and GLDAS products at the 50 km and 100 km scales suggests that these products achieve more reliable performance at coarse spatial resolutions. This finding underscores the importance of

considering spatial scale when selecting remote sensing SSM products for large-scale soil moisture assessments, as larger scales may provide a more consistent and accurate representation of soil moisture dynamics.

5.3. Considerations of Triple Collocation Analysis and future research

In recent years, the TCA has been widely used to evaluate the satellite-based and model-based SSM products (Leroux et al. 2011; Lyu et al. 2018; Xie et al. 2022; Xu et al. 2021). The TCA was applied to evaluate SMAP, ASCAT, ESA/CCI, and GLDAS SSM independently from in-situ SSM measurements. However, the error estimated by TCA does not represent the absolute error. TCA is applied to triplets of SSM data and this choice has significant impact on estimated errors, as shown by e.g. Kim et al. (2020) (Kim et al. 2020). We assessed this impact by applying TCA to four different triplets and by correlating the $RMSE_{TCA}$ estimated by TCA with RMSE estimated by comparing SSM data products with the corresponding in-situ measurements. Global error maps of SMAP, ASCAT, ESA/CCI, and GLDAS SSM products across Triplet 1–4 indicated that the SMAP SSM product had better performance, i.e. 74% of values had $RMSE_{TCA}$ values < 0.05 cm^3/cm^3, than ASCAT and ESA/CCI SSM products. On the other hand, the linear regression analysis of $RMSE_{TCA}$ values estimated by TCA and RMSE values estimated using in-situ SSM measurements showed a rather variable correlation, dependent on the composition of evaluated triplets. For instance, a linear correlation was found between $RMSE_{TCA}$ and RMSE values of SMAP SSM product in Triplet 1 with a correlation coefficient of 0.674, while the correlation was 0.199 for Triplet 2 (Figure 9). Thes findings confirm the need for in-situ SSM measurements to evaluate SSM data products.

This study led to identify three perspectives for a near-future follow-up of this study. 1) The ranking of remote sensing SSM data products. The results clearly show that no single data product performs best in all cases. However, the multiple evaluations can be used to propose a scoring system. Considering the numerous combinations of SSM products, in-situ measurements and error metrics presented in Table 5, we proposed to apply thresholds to identify instances of good performance, then counted the number of such instances for each data product. The setting of thresholds and the assessment of performance scores clearly require further study, but this approach is promising given the complex, multi-indicators evaluations involved. 2) The use of errors estimated by TCA. Zheng et al. (2022) indicated that the estimated $RMSE_{TCA}$ based on the TCA method could be adjusted to the true 'RMSE' values estimated using the results of the correlation analysis as applied in this study (Figure 9) (Zheng et al. 2022). Given the dependence on the composition of triplets and of the variables in correlation, the feasibility of this approach requires further study. 3) The next research will also include a detailed analysis of the performance of remote sensing SSM products across different seasons, plant types (e.g. grasslands vs. forests), and climates. And, it will involve assessing how well the products capture seasonal trends, extremes, or temporal variability. By focusing on specific cases of low and high variability in soil moisture, it will provide deeper insights into the strengths and limitations of current remote sensing products.

6. Conclusions

This study performed a comprehensive evaluation of four prominent global daily SSM products – SMAP (passive microwave), ASCAT (active microwave), ESA/CCI (merged active and passive microwave), and GLDAS (model simulation) – across various spatial scales (9/10 km, 25 km, 50 km, 100 km, and global-scale) using a new approach (Figure 3) in section 3 of this study. This evaluation aimed to quantify effect of footprint mismatch with in-situ measurements for SMAP, ASCAT, ESA/CCI and GLDAS SSM data products at different spatial scales. The ensuing key findings can be summarised as follows:

This study revealed significant seasonal and spatial variability in in-situ measurements across different spatial scales. In the CTP_SMTMN, SMN-SDR, and MAQU networks located in the

northern hemisphere, SSM peaked in summer (August) and reached its lowest levels in winter (December), with maximum values varying across regions, reflecting differences in seasonality. Additionally, the REMEDHUS network displayed pronounced spatial heterogeneity, particularly at smaller scales (10 km), indicating that upscaling from a limited number of sites may not accurately represent broader spatial grids. In contrast, the HOBE, OZNET, and SASMAS networks exhibited minimal seasonal variation and less pronounced differences across scales. The analysis of CV statistics further highlighted the spatial heterogeneity of in-situ measurements across scales, with CV values reaching approximately 15.9% and 44% in the CTP_SMTMN and REMEDHUS networks, respectively. These findings underscore the importance of considering spatial scale when evaluating soil moisture dynamics. The CV index effectively captured the spatial differential characteristics of in-situ SSM measurements across various scales, aiding in the assessment of the reliability of these measurements for validating remote sensing products such as ASCAT, SMAP, ESA/CCI, and GLDAS.

Comparing between CDF shapes of in-situ measured SSM across different spatial scales (i.e. 9/10 km, 25 km, 50 km, and 100 km) revealed a high degree of similarity within the same in-situ SSM observation network. The variability captured by in-situ SSM measurements appears to be comparable to that of remote sensing SSM data products, as indicated by the similar CDFs across various spatial resampling scales. For instance, in the CTP_SMTMN network, when in-situ SSM measurements were around 0.3 cm^3/cm^3, the CDF values across all four scales were nearly identical, and the slopes of four CDF curves showed only slight variations (0.0369, 0.0316, 0.0302, and 0.0302). Similarly, CDFs of remote sensing SSM products (SMAP, ASCAT, ESA/CCI, and GLDAS) exhibited comparable shapes within the same in-situ network. However, the study also revealed notable differences between the in-situ measurements and remote sensing SSM product data, particularly at larger spatial scales. Thus, while there in-situ measurements and remote sensing data products captured similar variability, there is still room for improvement in the accuracy of the latter.

The average MAE, RMSE, and Bias values for SMAP SSM product at 50 km and 100 km were the lowest, recorded at 0.052 cm^3/cm^3, 0.064 cm^3/cm^3, and 0.019 cm^3/cm^3, respectively. In the CTP_SMTMN network, the highest R value (0.904) was observed between the SMAP SSM product with100 km scale and in-situ measured measurements. Most $RMSE_{TCA}$ values of SMAP SSM product were below 0.05 cm^3/cm^3, indicating strong consistency with in-situ measurements. Overall, based on both metric-based evaluation using in-situ measurements and the TCA method, SMAP SSM product demonstrated the best consistency with in-situ measurements, and followed by ESA/CCI product. Additionally, the statistical analysis and box-plots revealed that the MAE for SMAP product in the REMEDHUS network nearly doubled between the 9 km and 100 km scales. Similarly, the ASCAT product in the SMN-SDR network showed a near doubling of MAE between the 10 km and 100 km scales. These findings suggest that the spatial resolution and coverage of remote sensing SSM products may not always perfectly align with the localised measurements, leading to discrepancies in the derived metrics. The impact of footprint mismatches between in-situ measurements and remote sensing SSM data, particularly for SMAP and ASCAT SSM products, was substantial, sometime resulting in metric differences nearly twice as large between smaller and large scales.

This study demonstrated that different combinations of remote sensing SSM products yielded markedly different evaluation results under various triplets. For instance, in Triplet 1 the correlation coefficient between the $RMSE_{TCA}$ and RMSE values was higher (0.674) compared to Triplet 2 (0.190) and Triplet 3 (0.472), indicating significant variability in accuracy assessments for the same remote sensing SSM product across different triplets. This suggest that relying on a single combination of remote sensing SSM products may not be ensure the robustness and feasibility of the TCA method. However, study also found certain correlations between the $RMSE_{TCA}$ values and the RMSE values based on in-situ measurements, which could be used to refine $RMSE_{TCA}$ maps. For example, in Triplet 1, the correlation (y = 0.805*x-0.005) was observed for SMAP product, while in Triplet 2, ASCAT product showed a correlation of y = 0.679*x + 0.028. In Triplet

3, the relationships were y = 0.254*x + 0.034 and y = 0.129*x + 0.002. These findings imply that such relationships might help to correct global $RMSE_{TCA}$ maps, thereby enhancing the reliability of remote sensing SSM product assessments.

Disclosure statement

No potential conflict of interest was reported by the author(s).

Data Availability Statement

The in-situ soil moisture measurement data used in this study were obtained from publicly available sources, including CTP_SMTMN, MAQU, SMN-SDR, HOBE, REMEDHUS, OZNET, and SASMAS networks, which can be accessed through the International Soil Moisture Network (https://ismn.geo.tuwien.ac.at/). The global-scale remote sensing surface soil moisture products (SMAP L3.0, ASCAT V3.0, ESA/CCI V7.1, and GLDAS V2.2) are available from their respective repositories: SMAP data from the National Aeronautics and Space Administration (NASA) (https://nsidc.org/data/smap), ASCAT data from the Copernicus Global Land Service (CGLS) system (https://land.copernicus.eu/global/products/swi), ESA/CCI data from the European Space Agency (https://esa-soilmoisture-cci.org/), and GLDAS data from the Goddard Earth Sciences Data and Information Services Center (GES DISC) of NASA (https://disc.gsfc.nasa.gov/). Any additional data related to this study are available from the corresponding author upon reasonable request.

References

Al-Yaari, A., J. P. Wigneron, W. Dorigo, A. Colliander, T. Pellarin, S. Hahn, A. Mialon, et al. 2019. "Assessment and Inter-Comparison of Recently Developed/Reprocessed Microwave Satellite Soil Moisture Products Using ISMN Ground-Based Measurements." *Remote Sensing of Environment* 224:289–303. https://doi.org/10.1016/j.rse.2019.02.008.

Al-Yaari, A., J. P. Wigneron, A. Ducharne, Y. Kerr, P. De Rosnay, R. De Jeu, A. Govind, et al. 2014. "Merging Two Passive Microwave Remote Sensing (SMOS and AMSR-E) Datasets to Produce a Long Term Record of Soil Moisture." International Geoscience and Remote Sensing Symposium (IGARSS), 2269–2272. https://doi.org/10.1109/IGARSS.2014.6946922.

Amini, Ata, Mehdi Karami Moghadam, Abdolnabi Abdeh Kolahchi, Mehrdad Raheli-Namin, and Kaywan Othman Ahmed. 2023. "Evaluation of GLDAS Soil Moisture Product over Kermanshah Province, Iran." *H2Open Journal* 6 (3): 373–386. https://doi.org/10.2166/h2oj.2023.057.

Bartalis, Zoltan, Wolfgang Wagner, Vahid Naeimi, Stefan Hasenauer, Klaus Scipal, Hans Bonekamp, Julia Figa, and Craig Anderson. 2007. "Initial Soil Moisture Retrievals from the METOP-A Advanced Scatterometer (ASCAT)." *Geophysical Research Letters*, https://doi.org/10.1029/2007GL031088.

Beck, Hylke E., Ming Pan, Diego G. Miralles, Rolf H. Reichle, Wouter A. Dorigo, Sebastian Hahn, Justin Sheffield, et al. 2021. "Evaluation of 18 Satellite- and Model-Based Soil Moisture Products Using in Situ Measurements from 826 Sensors." *Hydrology and Earth System Sciences* 25 (1): 17–40. https://doi.org/10.5194/hess-25-17-2021.

Bircher, S., N. Skou, K. H. Jensen, J. P. Walker, and L. Rasmussen. 2012. "A Soil Moisture and Temperature Network for SMOS Validation in Western Denmark." *Hydrology and Earth System Sciences* 16 (5): 1445–1463. https://doi.org/10.5194/hess-16-1445-2012.

Brocca, L., S. Hasenauer, T. Lacava, F. Melone, T. Moramarco, W. Wagner, W. Dorigo, et al. 2011. "Soil Moisture Estimation through ASCAT and AMSR-E Sensors: An Intercomparison and Validation Study across Europe." *Remote Sensing of Environment* 115 (12): 3390–3408. https://doi.org/10.1016/j.rse.2011.08.003.

Brocca, L., F. Melone, T. Moramarco, and R. Morbidelli. 2010. "Spatial-Temporal Variability of Soil Moisture and Its Estimation across Scales." *Water Resources Research*, https://doi.org/10.1029/2009WR008016.

Brocca, L., T. Tullo, F. Melone, T. Moramarco, and R. Morbidelli. 2012. "Catchment Scale Soil Moisture Spatial-Temporal Variability." *Journal of Hydrology*, https://doi.org/10.1016/j.jhydrol.2011.12.039.

Cai, Junjie, Bingting Zhou, Shiyan Chen, Xuelin Wang, Shuyun Yang, Zhiqing Cheng, Fengwen Wang, Xueying Mei, and Dong Wu. 2024. "Spatial and Temporal Variability of Soil Moisture and Its Driving Factors in the Northern Agricultural Regions of China." *Water (Switzerland)*, https://doi.org/10.3390/w16040556.

Ceballos, Antonio, Klaus Scipal, Wolfgang Wagner, and José Martínez-Fernández. 2005. "Validation of ERS Scatterometer-Derived Soil Moisture Data in the Central Part of the Duero Basin, Spain." *Hydrological Processes* 19 (8): 1549–1566. https://doi.org/10.1002/hyp.5585.

Chen, Fan, Wade T. Crow, Rajat Bindlish, Andreas Colliander, Mariko S. Burgin, Jun Asanuma, and Kentaro Aida. 2018. "Global-Scale Evaluation of SMAP, SMOS and ASCAT Soil Moisture Products Using Triple Collocation." *Remote Sensing of Environment* 214 (November 2017): 1–13. https://doi.org/10.1016/j.rse.2018.05.008.

Colliander, A., A. Berg, D. D. Bosch, T. Caldwell, J.-C. Calvet, and C. Holifield Collins. 2021. "Validation of Soil Moisture Data Products from the NASA SMAP Mission." *IEEE Journal of Selected Topics in Applied Earth Observations and Remote Sensing* 15 (June): 364–392. https://doi.org/10.36227/techrxiv.14714571.v1.

Colliander, A., T. J. Jackson, S. K. Chan, P. O'Neill, R. Bindlish, M. H. Cosh, T. Caldwell, et al. 2018. "An Assessment of the Differences between Spatial Resolution and Grid Size for the SMAP Enhanced Soil Moisture Product over Homogeneous Sites." *Remote Sensing of Environment* 207 (January): 65–70. https://doi.org/10.1016/j.rse.2018.02.006.

Cui, Chenyang, Jia Xu, Jiangyuan Zeng, Kun Shan Chen, Xiaojing Bai, Hui Lu, Quan Chen, and Tianjie Zhao. 2018. "Soil Moisture Mapping from Satellites: An Intercomparison of SMAP, SMOS, FY3B, AMSR2, and ESA CCI over Two Dense Network Regions at Different Spatial Scales." *Remote Sensing* 10 (33): 1–19. https://doi.org/10.3390/rs10010033.

Cui, Yaokui, Chao Zeng, Jie Zhou, Hongjie Xie, Wei Wan, Ling Hu, Wentao Xiong, Xi Chen, Wenjie Fan, and Yang Hong. 2019. "A Spatio-Temporal Continuous Soil Moisture Dataset over the Tibet Plateau from 2002–2015." *Scientific Data* 6 (1): 247. https://doi.org/10.1038/s41597-019-0228-x.

Dorigo, Wouter, Irene Himmelbauer, Daniel Aberer, Lukas Schremmer, Ivana Petrakovic, Luca Zappa, Wolfgang Preimesberger, et al. 2021. "The International Soil Moisture Network: Serving Earth System Science for over a Decade." *Hydrology and Earth System Sciences* 25 (11): 5749–5804. https://doi.org/10.5194/hess-25-5749-2021.

Dorigo, W. A., K. Scipal, R. M. Parinussa, Y. Y. Liu, W. Wagner, R. A. M. De Jeu, and V. Naeimi. 2010. "Error Characterisation of Global Active and Passive Microwave Soil Moisture Datasets." *Hydrology and Earth System Sciences* 14 (12): 2605–2616. https://doi.org/10.5194/hess-14-2605-2010.

Dorigo, Wouter, Wolfgang Wagner, Clement Albergel, Franziska Albrecht, Gianpaolo Balsamo, Luca Brocca, Daniel Chung, et al. 2017. "ESA CCI Soil Moisture for Improved Earth System Understanding: State-of-the Art and Future Directions." *Remote Sensing of Environment* 203:185–215. https://doi.org/10.1016/j.rse.2017.07.001.

Dorigo, W. A., W. Wagner, R. Hohensinn, S. Hahn, C. Paulik, A. Xaver, A. Gruber, et al. 2011. "The International Soil Moisture Network: A Data Hosting Facility for Global in Situ Soil Moisture Measurements." *Hydrology and Earth System Sciences* 15 (5): 1675–1698. https://doi.org/10.5194/hess-15-1675-2011.

Entekhabi, Dara, Eni G. Njoku, Peggy E. O'Neill, Kent H. Kellogg, Wade T. Crow, Wendy N. Edelstein, Jared K. Entin, et al. 2010. "The Soil Moisture Active Passive (SMAP) Mission." Proceedings of the IEEE 98 (5): 704–716. https://doi.org/10.1109/JPROC.2010.2043918.

Figa-Saldana, J., JJW Wilson, E Attema, R Gelsthorpe, M. R. Gelsthorpe, and A. Stoffelen. 2002. "The Advanced Scatterometer (ASCAT) on the Meteorological Operational (MetOp) Platform: A Follow on for European Wind Scatterometers." *Canadian Journal of Remote Sensing* 28 (3): 404–412. https://doi.org/10.5589/m02-035.

González-Zamora, Ángel, Nilda Sánchez, José Martínez-Fernández, Ángela Gumuzzio, María Piles, and Estrella Olmedo. 2015. "Long-Term SMOS Soil Moisture Products: A Comprehensive Evaluation across Scales and Methods in the Duero Basin (Spain)." *Physics and Chemistry of the Earth* 83–84:123–136. https://doi.org/10.1016/j.pce.2015.05.009.

González-Zamora, Á, N. Sánchez, M. Pablos, and J. Martínez-Fernández. 2019. "CCI Soil Moisture Assessment with SMOS Soil Moisture and in Situ Data under Different Environmental Conditions and Spatial Scales in Spain." *Remote Sensing of Environment* 225 (March 2017): 469–482. https://doi.org/10.1016/j.rse.2018.02.010.

Gruber, A., G. De Lannoy, C. Albergel, A. Al-Yaari, L. Brocca, J. C. Calvet, A. Colliander, et al. 2020. "Validation Practices for Satellite Soil Moisture Retrievals: What Are (the) Errors?" *Remote Sensing of Environment* 244 (September 2019): 111806. https://doi.org/10.1016/j.rse.2020.111806.

Gruber, Alexander, Wouter Arnoud Dorigo, Wade Crow, and Wolfgang Wagner. 2017. "Triple Collocation-Based Merging of Satellite Soil Moisture Retrievals." *IEEE Transactions on Geoscience and Remote Sensing* 55 (12): 6780–6792. https://doi.org/10.1109/TGRS.2017.2734070.

Gruber, A., W. A. Dorigo, S. Zwieback, A. Xaver, and W. Wagner. 2013. "Characterizing Coarse-Scale Representativeness of in Situ Soil Moisture Measurements from the International Soil Moisture Network." *Vadose Zone Journal* 12 (2): 1–16. https://doi.org/10.2136/vzj2012.0170.

Gruber, A., C.-H. Su, S. Zwieback, W. Crow, W. Dorigo, and W. Wagner. 2016. "Recent Advances in (Soil Moisture) Triple Collocation Analysis." *International Journal of Applied Earth Observation and Geoinformation* 45:200–211. https://doi.org/10.1016/j.jag.2015.09.002.

Herbert, Christoph, Miriam Pablos, Mercè Vall-llossera, Adriano Camps, and José Martínez-Fernández. 2020. "Analyzing Spatio-Temporal Factors to Estimate the Response Time between SMOS and in-Situ Soil Moisture at Different Depths." *Remote Sensing* 12 (16), https://doi.org/10.3390/RS12162614.

Hu, Fengmin, Zushuai Wei, Xining Yang, Wenjun Xie, Yuanxi Li, Changlu Cui, Beibei Yang, Chongxin Tao, Wen Zhang, and Lingkui Meng. 2022. "Assessment of SMAP and SMOS Soil Moisture Products Using Triple Collocation Method over Inner Mongolia." *Journal of Hydrology: Regional Studies* 40 (September 2021): 101027. https://doi.org/10.1016/j.ejrh.2022.101027.

Jackson, Thomas J. 1993. "Measuring Surface Soil Moisture Using Passive Microwave Remote Sensing." *Hydrological Processes* 7 (2): 139–152. https://doi.org/10.1002/hyp.3360070205.

Jackson, T. J., P. O'Neill, E. Njoku, S. Chan, R. Bindlish, A. Colliander, F. Chen, et al. 2016. "Calibration and Validation for the L2/3_SM_P Version 3 Data Products," 1–44.

Jalilibal, Zahra, Amirhossein Amiri, Philippe Castagliola, and Michael B.C. Khoo. 2021. "Monitoring the Coefficient of Variation: A Literature Review." *Computers and Industrial Engineering*, https://doi.org/10.1016/j.cie.2021.107600.

Jensen, Karsten H., and Tissa H. Illangasekare. 2011. "HOBE: A Hydrological Observatory." *Vadose Zone Journal* 10 (1): 1–7. https://doi.org/10.2136/vzj2011.0006.

Karthikeyan, L., Ming Pan, Niko Wanders, D. Nagesh Kumar, and Eric F. Wood. 2017a. "Four Decades of Microwave Satellite Soil Moisture Observations: Part 2. Product Validation and Inter-Satellite Comparisons." *Advances in Water Resources* 109:236–252. https://doi.org/10.1016/j.advwatres.2017.09.010.

Karthikeyan, L., Ming Pan, Niko Wanders, D. Nagesh Kumar, and Eric F. Wood. 2017b. "Four Decades of Microwave Satellite Soil Moisture Observations: Part 1. A Review of Retrieval Algorithms." *Advances in Water Resources* 109:106–120. https://doi.org/10.1016/j.advwatres.2017.09.006.

Kerr, Y. H., J. P. Wigneron, A. Al Bitar, A. Mialon, and P. K. Srivastava. 2016. "Soil Moisture from Space: Techniques and Limitations." In *Satellite Soil Moisture Retrieval: Techniques and Applications*, 3–27. Elsevier Inc. https://doi.org/10.1016/B978-0-12-803388-3.00001-2.

Kim, Seokhyeon, Jianzhi Dong, and Ashish Sharma. 2021a. "A Triple Collocation-Based Comparison of Three L-Band Soil Moisture Datasets, SMAP, SMOS-IC, and SMOS, Over Varied Climates and Land Covers." *Frontiers in Water* 3 (December), https://doi.org/10.3389/frwa.2021.693172.

Kim, Hyunglok, Sangchul Lee, Michael H. Cosh, Venkataraman Lakshmi, Yonghwan Kwon, and Gregory W. McCarty. 2021b. "Assessment and Combination of SMAP and Sentinel-1A/B-Derived Soil Moisture Estimates with Land Surface Model Outputs in the Mid-Atlantic Coastal Plain, USA." *IEEE Transactions on Geoscience and Remote Sensing* 59 (2): 991–1011. https://doi.org/10.1109/TGRS.2020.2991665.

Kim, Hyunglok, Robert Parinussa, Alexandra G. Konings, Wolfgang Wagner, Michael H. Cosh, Venkat Lakshmi, Muhammad Zohaib, and Minha Choi. 2018. "Global-Scale Assessment and Combination of SMAP with ASCAT (Active) and AMSR2 (Passive) Soil Moisture Products." *Remote Sensing of Environment* 204:260–275. https://doi.org/10.1016/j.rse.2017.10.026.

Kim, Seokhyeon, Robert M. Parinussa, Yi Y. Liu, Fiona M. Johnson, and Ashish Sharma. 2016. "Merging Alternate Remotely-Sensed Soil Moisture Retrievals Using a Non-Static Model Combination Approach." *Remote Sensing* 8 (6): 1–16. https://doi.org/10.3390/rs8060518.

Kim, Seokhyeon, Hung T. Pham, Yi Y. Liu, Lucy Marshall, and Ashish Sharma. 2020. "Improving the Combination of Satellite Soil Moisture Data Sets by Considering Error Cross Correlation: A Comparison Between Triple Collocation (TC) and Extended Double Instrumental Variable (EIVD) Alternatives." *IEEE Transactions on Geoscience and Remote Sensing* 59 (9): 7285–7295. https://doi.org/10.1109/tgrs.2020.3032418.

Kolahchi, Abdolnabi Abdeh, Morteza Miri, Mehran Zand. 2024. Comparative Evaluation of GLDAS , ESA CCI SM and SMAP Soil Moisture with in Situ Measurements (Case Study: Lorestan Province)." 2023. https://doi.org/10.22034/EWE.2023.367471.1819.

Leroux, D. J., Y. H. Kerr, P. Richaume, and B. Berthelot. 2011. "Estimating SMOS Error Structure Using Triple Collocation." International Geoscience and Remote Sensing Symposium (IGARSS), 24–27.

Li, Changming, Guoqiang Tang, and Yang Hong. 2018. "Cross-Evaluation of Ground-Based, Multi-Satellite and Reanalysis Precipitation Products: Applicability of the Triple Collocation Method across Mainland China." *Journal of Hydrology* 562:71–83. https://doi.org/10.1016/j.jhydrol.2018.04.039.

Liu, Y. Y., W. A. Dorigo, R. M. Parinussa, R. A. M. De Jeu, W. Wagner, M. F. Mccabe, J. P. Evans, and A. I. J. M. Van Dijk. 2012. "Trend-Preserving Blending of Passive and Active Microwave Soil Moisture Retrievals." *Remote Sensing of Environment* 123: 280–297. https://doi.org/10.1016/j.rse.2012.03.014.

Liu, Y. Y., R. M. Parinussa, W. A. Dorigo, R. A. M. De Jeu, W. Wagner, A. I. J. M. Van Dijk, M. F. McCabe, and J. P. Evans. 2011. "Developing an Improved Soil Moisture Dataset by Blending Passive and Active Microwave Satellite-Based Retrievals." *Hydrology and Earth System Sciences* 15 (2): 425–436. https://doi.org/10.5194/hess-15-425-2011.

Liu, Yangxiaoyue, Yuke Zhou, Ning Lu, Ronglin Tang, Naijing Liu, Yong Li, Ji Yang, Wenlong Jing, and Chenghu Zhou. 2021. "Comprehensive Assessment of Fengyun-3 Satellites Derived Soil Moisture with in-Situ Measurements across the Globe." *Journal of Hydrology* 594 (December 2020): 125949. https://doi.org/10.1016/j.jhydrol.2020.125949.

Lu, Xinyu, Guoqiang Tang, Xinchun Liu, Xiuqin Wang, Yan Liu, and Ming Wei. 2021. "The Potential and Uncertainty of Triple Collocation in Assessing Satellite Precipitation Products in Central Asia." *Atmospheric Research* 252 (October 2020): 105452. https://doi.org/10.1016/j.atmosres.2021.105452.

Lyu, Haobo, Kaighin A. McColl, Xinlu Li, Chris Derksen, Aaron Berg, T. Andrew Black, Eugenie Euskirchen, et al. 2018. "Validation of the SMAP Freeze/Thaw Product Using Categorical Triple Collocation." *Remote Sensing of Environment* 205 (November 2017): 329–337. https://doi.org/10.1016/j.rse.2017.12.007.

Ma, Hongliang, Jiangyuan Zeng, Nengcheng Chen, Xiang Zhang, Michael H. Cosh, and Wei Wang. 2019. "Satellite Surface Soil Moisture from SMAP, SMOS, AMSR2 and ESA CCI: A Comprehensive Assessment Using Global Ground-Based Observations." *Remote Sensing of Environment* 231:111215. https://doi.org/10.1016/j.rse.2019.111215.

Mahmood, Rezaul, Ashley Littell, Kenneth G. Hubbard, and Jinsheng You. 2012. "Observed Data-Based Assessment of Relationships among Soil Moisture at Various Depths, Precipitation, and Temperature." *Applied Geography* 34:255–264. https://doi.org/10.1016/j.apgeog.2011.11.009.

Martínez-Fernández, J., and A. Ceballos. 2005. "Mean Soil Moisture Estimation Using Temporal Stability Analysis." *Journal of Hydrology* 312 (1-4): 28–38. https://doi.org/10.1016/j.jhydrol.2005.02.007.

McColl, Kaighin A., Jur Vogelzang, Alexandra G. Konings, Dara Entekhabi, María Piles, and Ad Stoffelen. 2014. "Extended Triple Collocation: Estimating Errors and Correlation Coefficients with Respect to an Unknown Target." *Geophysical Research Letters* 41 (17): 6229–6236. https://doi.org/10.1002/2014GL061322.

Menenti, Massimo, Xin Li, Li Jia, Kun Yang, Francesca Pellicciotti, Marco Mancini, Jiancheng Shi, et al. 2021. "Multi-Source Hydrological Data Products to Monitor High Asian River Basins and Regional Water Security." *Remote Sensing* 13 (24), https://doi.org/10.3390/rs13245122.

Meng, Fanhao, Min Luo, Chula Sa, Mulan Wang, and Yuhai Bao. 2022. "Quantitative Assessment of the Effects of Climate, Vegetation, Soil and Groundwater on Soil Moisture Spatiotemporal Variability in the Mongolian Plateau." *Science of the Total Environment* 809:152198. https://doi.org/10.1016/j.scitotenv.2021.152198.

Miralles, Diego G., Wade T. Crow, and Michael H. Cosh. 2010. "Estimating Spatial Sampling Errors in Coarse-Scale Soil Moisture Estimates Derived from Point-Scale Observations." *Journal of Hydrometeorology* 11 (6): 1423–1429. https://doi.org/10.1175/2010JHM1285.1.

Mohanty, Binayak P., Michael H. Cosh, Venkat Lakshmi, and Carsten Montzka. 2017. "Soil Moisture Remote Sensing: State-of-the-Science." *Vadose Zone Journal* 16 (1): 1–9. https://doi.org/10.2136/vzj2016.10.0105.

Nichols, Sue. 2011. "Review and Evaluation of Remote Sensing Methods for Soil-Moisture Estimation." *Journal of Photonics for Energy* 2 (1): 028001. https://doi.org/10.1117/1.3534910.

Njoku, Eni G., and Steven K. Chan. 2006. "Vegetation and Surface Roughness Effects on AMSR-E Land Observations." *Remote Sensing of Environment* 100 (2): 190–199. https://doi.org/10.1016/j.rse.2005.10.017.

Owe, M., R. De Jeu, and J. Walker. 2001. "A Methodology for Surface Soil Moisture and Vegetation Optical Depth Retrieval Using the Microwave Polarization Difference Index." *IEEE Transactions on Geoscience and Remote Sensing* 39 (8): 1643–1654. https://doi.org/10.1109/36.942542.

Pandey, Vanita, and Pankaj K. Pandey. 2010. "Spatial and Temporal Variability of Soil Moisture." *International Journal of Geosciences*, https://doi.org/10.4236/ijg.2010.12012.

Piles, Maria, Joaquim Ballabrera-Poy, and Joaquín Muñoz-Sabater. 2019. "Dominant Features of Global Surface Soil Moisture Variability Observed by the SMOS Satellite." *Remote Sensing* 11 (1): 1–21. https://doi.org/10.3390/rs11010095.

Qin, Jun, Kun Yang, Ning Lu, Yingying Chen, Long Zhao, and Menglei Han. 2013. "Spatial Upscaling of In-Situ Soil Moisture Measurements Based on MODIS-Derived Apparent Thermal Inertia." *Remote Sensing of Environment* 138 (October 2017): 1–9. https://doi.org/10.1016/j.rse.2013.07.003.

Ray, Ram L., Ali Fares, Yiping He, and Marouane Temimi. 2017. "Evaluation and Inter-Comparison of Satellite Soil Moisture Products Using in Situ Observations over Texas, U.S." *Water (Switzerland)* 9 (6), https://doi.org/10.3390/w9060372.

Rodell, Matthew, P. R. Houser, U. Jambor, J. Gottschalck, K. Mitchell, C. J. Meng, K. Arsenault, et al. 2004. "The Global Land Data Assimilation System." *Bulletin of the American Meteorological Society* 85 (3): 381–394. https://doi.org/10.1175/BAMS-85-3-381.

Rüdiger, Christoph, Greg Hancock, Herbert M. Hemakumara, Barry Jacobs, Jetse D. Kalma, Cristina Martinez, Mark Thyer, Jeffrey P. Walker, Tony Wells, and Garry R. Willgoose. 2007. "Goulburn River Experimental Catchment Data Set." *Water Resources Research* 43 (10): W10403. https://doi.org/10.1029/2006WR005837.

Saeedi, Mohammad, Sina Nabaei, Hyunglok Kim, Ameneh Tavakol, and Venkataraman Lakshmi. 2023. "Performance Assessment of SM2RAIN-NWF Using ASCAT Soil Moisture via Supervised Land Cover-Soil-Climate Classification." *Remote Sensing of Environment* 285 (April 2022): 113393. https://doi.org/10.1016/j.rse.2022.113393.

Sánchez, N., A. González-Zamora, J. Martínez-Fernández, and M. Pablos. 2018. "Upscaling Ground Soil Moisture to Validate Remote Sensing Estimations: Is the Simple Spatial Average a Suitable Approach?" International Geoscience and Remote Sensing Symposium (IGARSS), 9122–9125.

Sánchez, Nilda, José Martínez-Fernádez, Anna Scaini, and Carlos Pérez-Gutierrez. 2012. "Validation of the SMOS L2 Soil Moisture Data in the REMEDHUS Network (Spain)." *IEEE Transactions on Geoscience and Remote Sensing* 50 (5 PART 1): 1602–1611. https://doi.org/10.1109/TGRS.2012.2186971.

Saxton, K. E., and W. J. Rawls. 2006. "Soil Water Characteristic Estimates by Texture and Organic Matter for Hydrologic Solutions." *Soil Science Society of America Journal* 70 (5): 1569–1578. https://doi.org/10.2136/sssaj2005.0117.

Seneviratne, Sonia I., Thierry Corti, Edouard L. Davin, Martin Hirschi, Eric B. Jaeger, Irene Lehner, Boris Orlowsky, and Adriaan J. Teuling. 2010. "Investigating Soil Moisture-Climate Interactions in a Changing Climate: A Review." *Earth-Science Reviews* 99 (3-4): 125–161. https://doi.org/10.1016/j.earscirev.2010.02.004.

Shi, Jiancheng, Lingmei Jiang, Lixin Zhang, K. S. Chen, Jean Pierre Wigneron, André Chanzy, and Thomas J. Jackson. 2006. "Physically Based Estimation of Bare-Surface Soil Moisture with the Passive Radiometers." *IEEE Transactions on Geoscience and Remote Sensing* 44 (11): 3145–3152. https://doi.org/10.1109/TGRS.2006.876706.

Singh, Abhilash, Kumar Gaurav, Ganesh Kumar Meena, and Shashi Kumar. 2020. "Estimation of Soil Moisture Applying Modified Dubois Model to Sentinel-1; A Regional Study from Central India." *Remote Sensing* 12 (14): 1–19. https://doi.org/10.3390/rs12142266.

Skøien, J. O., G. Blöschl, and A. W. Western. 2003. "Characteristic Space Scales and Timescales in Hydrology." *Water Resources Research* 39 (10), https://doi.org/10.1029/2002WR001736.

Smith, A. B., J. P. Walker, A. W. Western, R. I. Young, K. M. Ellett, R. C. Pipunic, R. B. Grayson, L. Siriwardena, F. H. S. Chiew, and H. Richter. 2012. "The Murrumbidgee Soil Moisture Monitoring Network Data Set." *Water Resources Research* 48 (7): 1–6. https://doi.org/10.1029/2012WR011976.

Su, Z., J. Wen, L. Dente, R. Van Der Velde, L. Wang, Y. Ma, K. Yang, and Z. Hu. 2011. "The Tibetan Plateau Observatory of Plateau Scale Soil Moisture and Soil Temperature (Tibet-Obs) for Quantifying Uncertainties in Coarse Resolution Satellite and Model Products." *Hydrology and Earth System Sciences* 15 (7): 2303–2316. https://doi.org/10.5194/hess-15-2303-2011.

Venegas-Cordero, Nelson, Cyrine Cherrat, Zbigniew W. Kundzewicz, Jitendra Singh, and Mikołaj Piniewski. 2023. "Model-Based Assessment of Flood Generation Mechanisms over Poland: The Roles of Precipitation, Snowmelt, and Soil Moisture Excess." *Science of the Total Environment* 891 (June), https://doi.org/10.1016/j.scitotenv.2023.164626.

Wagner, Wolfgang, Sebastian Hahn, Thomas Melzer, T. U. Wien, See Profile, Zoltan Bartalis, Richard Kidd, et al. 2013. "The ASCAT Soil Moisture Product: A Review of Its." *Researchgate.Net* 22 (1): 5–33. https://doi.org/10.1127/0941-2948/2013/0399.

Wagner, Wolfgang, Guido Lemoine, and Helmut Rott. 1999. "A Method for Estimating Soil Moisture from ERS Scatterometer and Soil Data." *Remote Sensing of Environment* 70 (2): 191–207. https://doi.org/10.1016/S0034-4257(99)00036-X.

Wang, Jingping, Xiaodan Wu, Rongqi Tang, Dujuan Ma, Qicheng Zeng, Qing Xiao, and Jianguang Wen. 2022a. "The First Assessment of Coarse-Pixel Soil Moisture Products within the Multi-Scale Validation Framework over Qinghai-Tibet Plateau." *Journal of Hydrology* 613 (PB): 128454. https://doi.org/10.1016/j.jhydrol.2022.128454.

Wang, Jingping, Xiaodan Wu, Rongqi Tang, Qicheng Zeng, Zheng Li, Jianguang Wen, and Qing Xiao. 2022b. "Evaluation of Three Error-Correction Models Based on the Matched Pixel Scale Ground 'Truth': A Case Study of MCD43A3 V006 Over the Heihe River Basin, China." *IEEE Journal of Selected Topics in Applied Earth Observations and Remote Sensing* 15:8785–8797. https://doi.org/10.1109/JSTARS.2022.3213184.

Wen, Xin, Hui Lu, Chengwei Li, Toshio Koike, and Ichirou Kaihotsu. 2014. "Inter-Comparison of Soil Moisture Products from SMOS, AMSR-E, ECWMF and GLDAS over the Mongolia Plateau." In *Land Surface Remote Sensing II*, 9260, 92600O, 1–8. Society of Photo-Optical Instrumentation Engineers. https://doi.org/10.1117/12.2068952.

Wen, Jianguang, Xiaodan Wu, Qing Xiao, Qinhuo Liu, Mingguo Ma, Xingming Zheng, Yonghua Qu, et al. 2023. "Full-Band, Multi-Angle, Multi-Scale, and Temporal Dynamic Field Spectral Measurements in China." *Scientific Data* 10 (1): 1–18. https://doi.org/10.1038/s41597-022-01899-x.

Weng, Baisha, Wuxia Bi, Zhixuan Zhao, Ting Xu, and Dengming Yan. 2018. "Spatial and Temporal Variability of Soil Moisture Based on Multifractal Analysis." *Arabian Journal of Geosciences*, https://doi.org/10.1007/s12517-018-3832-8.

Wigneron, J. P., Y. Kerr, P. Waldteufel, K. Saleh, M. J. Escorihuela, P. Richaume, P. Ferrazzoli, et al. 2007. "L-Band Microwave Emission of the Biosphere (L-MEB) Model: Description and Calibration against Experimental Data Sets over Crop Fields." *Remote Sensing of Environment* 107 (4): 639–655. https://doi.org/10.1016/j.rse.2006.10.014.

Wu, Kai, Dongryeol Ryu, Lei Nie, and Hong Shu. 2021. "Time-Variant Error Characterization of SMAP and ASCAT Soil Moisture Using Triple Collocation Analysis." *Remote Sensing of Environment* 256 (December 2020): 112324. https://doi.org/10.1016/j.rse.2021.112324.

Xie, Qiuxia, Li Jia, Qiting Chen, Yanmin Yin, and Massimo Menenti. 2021. "Evaluation of Microwave Remote Sensing Soil Moisture Products in Farming-Pastoral Area of Shandian River Basin." *National Remote Sensing Bulletin* 25 (4): 974–989. https://doi.org/10.11834/jrs.20219491.

Xie, Qiuxia, Li Jia, Massimo Menenti, and Guangcheng Hu. 2022. "Global Soil Moisture Data Fusion by Triple Collocation Analysis from 2011 to 2018." *Scientific Data* 9 (1): 1–19. https://doi.org/10.1038/s41597-021-01104-5.

Xing, Zanpin, Lei Fan, Lin Zhao, Gabrielle De Lannoy, Frédéric Frappart, Jian Peng, Xiaojun Li, et al. 2021. "A First Assessment of Satellite and Reanalysis Estimates of Surface and Root-Zone Soil Moisture over the Permafrost Region of Qinghai-Tibet Plateau." *Remote Sensing of Environment* 265 (March), https://doi.org/10.1016/j.rse.2021.112666.

Xu, Lei, Nengcheng Chen, Xiang Zhang, Hamid Moradkhani, Chong Zhang, and Chuli Hu. 2021. "In-Situ and Triple-Collocation Based Evaluations of Eight Global Root Zone Soil Moisture Products." *Remote Sensing of Environment* 254 (December 2020): 112248. https://doi.org/10.1016/j.rse.2020.112248.

Yang, Kun, Jun Qin, Long Zhao, Yingying Chen, Wenjun Tang, Menglei Han, La Zhu, et al. 2013. "A Multiscale Soil Moisture and Freeze-Thaw Monitoring Network on the Third Pole." *Bulletin of the American Meteorological Society* 94 (12): 1907–1916. https://doi.org/10.1175/BAMS-D-12-00203.1.

Yao, Panpan, Hui Lu, Jiancheng Shi, Tianjie Zhao, Kun Yang, Michael H. Cosh, Daniel J.Short Gianotti, and Dara Entekhabi. 2021. "A Long Term Global Daily Soil Moisture Dataset Derived from AMSR-E and AMSR2 (2002-2019)." *Scientific Data* 8 (1): 1–17. https://doi.org/10.1038/s41597-021-00925-8.

Young, Rodger, Jeffrey P. Walker, Nicholas Yeoh, Adam Smith, Kevin Ellett, Olivier Merlin, and Andrew W. Western. 2008. *Soil Moisture and Meteorological Observations from the Murrumbidgee Catchment.* http://www.oznet.org.au/documentation/.

Zeng, Jiangyuan, Zhen Li, Quan Chen, Haiyun Bi, Jianxiu Qiu, and Pengfei Zou. 2015. "Evaluation of Remotely Sensed and Reanalysis Soil Moisture Products over the Tibetan Plateau Using In-Situ Observations." *Remote Sensing of Environment* 163:91–110. https://doi.org/10.1016/j.rse.2015.03.008.

Zhao, Tianjie, Jiancheng Shi, Liqing Lv, Hongxin Xu, Deqing Chen, Qian Cui, Thomas J Jackson, et al. 2020. "Soil Moisture Experiment in the Luan River Supporting New Satellite Mission Opportunities." *Remote Sensing of Environment* 240:111680. https://doi.org/10.1016/j.rse.2020.111680.

Zhao, Long, Kun Yang, Jun Qin, Yingying Chen, Wenjun Tang, Hui Lu, and Zong Liang Yang. 2014. "The Scale-Dependence of SMOS Soil Moisture Accuracy and Its Improvement through Land Data Assimilation in the Central Tibetan Plateau." *Remote Sensing of Environment* 152:345–355. https://doi.org/10.1016/j.rse.2014.07.005.

Zhao, Long, Kun Yang, Jun Qin, Yingying Chen, Wenjun Tang, Carsten Montzka, Hui Wu, Changgui Lin, Menglei Han, and Harry Vereecken. 2013. "Spatiotemporal Analysis of Soil Moisture Observations within a Tibetan Mesoscale Area and Its Implication to Regional Soil Moisture Measurements." *Journal of Hydrology* 482:92–104. https://doi.org/10.1016/j.jhydrol.2012.12.033.

Zheng, Jingyao, Tianjie Zhao, Haishen Lü, Jiancheng Shi, Michael H. Cosh, Dabin Ji, Lingmei Jiang, et al. 2022. "Assessment of 24 Soil Moisture Datasets Using a New in Situ Network in the Shandian River Basin of China." *Remote Sensing of Environment* 271, https://doi.org/10.1016/j.rse.2022.112891.

Zwieback, Simon, Chun Hsu Su, Alexander Gruber, Wolfgang Wagner, and Wouter A. Dorigo. 2016. "The Impact of Quadratic Nonlinear Relations between Soil Moisture Products on Uncertainty Estimates from Triple Collocation Analysis and Two Quadratic Extensions." *Journal of Hydrometeorology* 17 (6): 1725–1743. https://doi.org/10.1175/JHM-D-15-0213.1.

Appendix A

1. Soil Moisture Active Passive (SMAP)

The SMAP mission, launched by National Aeronautics and Space Administration (NASA) in January 2015, began collecting data in April of the same year, specifically for acquiring SSM measurements (Entekhabi et al. 2010). The SMAP satellite operates in a near-polar and sun-synchronous orbit is equipped with two low-frequency microwave remote sensors: an L-band radar (1.26 GHz) and an L-band radiometer (1.41 GHz) with a 40° incidence angle (Entekhabi et al. 2010). The satellite crosses the equator approximately 06:00 and 18:00 local time, allowing global coverage every 1–3 days. Currently, SMAP offers a wide range of soil moisture products (SSM) across multiple levels, including L2, L3, and L4 products. These products are available at various spatial resolutions such as 3 , 9 , and 36 km, and include radar, radiometer, and combined data (Colliander et al. 2021). However, the 3 km data are only about

three months due to the L-band radar malfunction (Jackson et al. 2016). Therefore, this study focuses on the long-term SMAP Level 3 SSM product with a 9 km spatial grid resolution (available from 2015 to present), accessible via https://nsidc.org/data or https://search.earthdata.nasa.gov/. The SMAP Level 3 SSM product is derived from Level 2 SSM data using the SCA-V for SSM retrieval algorithm, applied at a 9 km spatial grid resolution.

2. Advanced Scatterometer (ASCAT)

ASCAT sensors, mounted on the Meteorological Operational A, B, and C (MetOp-A, – B, and – C) satellites launched by ESA in 2006, 2012, and 2018, respectively, are active microwave instruments operating at C-band (5.3 GHz, wavelength = 5.7 cm) with vertical polarisation (Figa-Saldana et al., 2002; Wagner et al. 2013). These sensors provide global radar backscatter data within 1∼3 days, passing over the equator at approximately 09:30 and 21:30 local time (Figa-Saldana et al., 2002). The global ASCAT product, available from 2007 to the present, is produced using a SWI-based soil moisture inversion algorithm developed by the Vienna University of Technology (Wagner et al. 2013, 1999). The product, with a spatial grid resolution of 0.1°, is available through the Copernicus Global Land Service (CGLS) system at https://land.copernicus.eu/global/products/swi. The unit of ASCAT product was expressed as the degree of saturation (%), not as volumetric soil water content (cm^3/cm^3). The ASCAT product includes eight layers utilising T values (1, 5, 10, 15, 20, 40, 60, and 100), each representing different soil depths (e.g. T-values from 1 to 100 correspond to increasing soil depths). This study utilises the first layer (T = 1), representing soil depths of 1–5 cm.

3. European Space Agency Climate Change Initiative (ESA/CCI)

The ESA/CCI V7.1 SSM product is part of the ESA's Soil Moisture Essential Climate Variable (ECV) Climate Change Initiative project, consisting of three fusion datasets created using the TCA-based Linear Weight Fusion (TCA-based LWF) method: the active, passive, and combined microwave SSM fusion datasets (Dorigo et al. 2017; Gruber et al. 2017; Liu et al. 2011). These datasets are freely available at https://esa-soilmoisture-cci.org/. The active (1991–2020) dataset includes data from the European Remote Sensing-1/2 (ERS-1/2) and ASCAT SSM products generated by the TU Wien soil moisture retrieval algorithm, while the passive dataset (1978–2020) includes data from several satellites i.e. the Nimbus-7's Scanning Multichannel Microwave Radiometer (SMMR), Special Sensor Microwave-Imager (SSM/I), Microwave Imager (TMI), AMSR-E, WindSat Radiometer (Windsat), AMSR-2, SMOS, SMAP, Global Precipitation Measurement (GPM), and FengYun3-B/C/D (FY3 – B/C/D) SSM products, all processed using the Land Parameter Retrieval Model (LPRM) algorithm. The combined soil moisture product merges the Level 2 active and passive microwave SSM products, offering a spatiotemporally continuous global dataset with daily 0.25°resolution from 1978–2020 (Liu et al. 2012, 2011). Due to its lower spatial-temporal gaps and higher accuracy, this study uses the combined ESA/CCI V7.1 product.

4. Global Land Data Assimilation System (GLDAS)

NASA's GLDAS project aims to generate optimal fields of land surface fluxes and states using land surface assimilation methods from satellite and ground observation data (Amini et al. 2023; Wen et al. 2014). Currently, the GLDAS Version 2 (GLDAS V2) dataset comprises three components (GLDAS V2.0, GLDAS V2.1, and GLDAS V2.2), covering from1948 to the present (GLDAS V2.0 covers from 1948–2014, GLDAS-2.1 from 2000 to the present, and GLDAS V2.2 from 2003 to the present) (Kolahchi, Miri, and Zand 2024; Rodell et al. 2004b). The GLDAS V2 datasets have three temporal resolutions (3-hourly, daily, and monthly) and two spatial grid resolutions (1.0° and 0.25°). Unlike GLDAS V2.0 and 2.1 (which lacked data assimilation), the current GLDAS V2.2 product incorporates data assimilation from the Gravity Recovery and Climate Experiment (GRACE) mission starting from 2003 to the present. This study selects the GLDAS V2.2 Catchment Land Surface Model (CLSM) product with a 0.25° resolution and daily temporal resolution, consistent with the ESA/CCI SSM product, focusing on soil moisture at a depth of 0–2 cm.